Mesoscale Aspects of Cyclogenesis

Lance F. Bosart

Department of Atmospheric Science

State University of New York at Albany

1400 Washington Avenue

Albany, New York 12222

U.S.A.

Summary: This paper reviews some mesoscale observational aspects of the cyclogenesis problem. It begins with some remarks on the Atlantic coastal storm of 22-23 February 1987. This storm, similar in some ways to the Presidents' Day storm of February 1979, was poorly forecast by the operational ECMWF model and the US Nested Grid Model (NGM). Somewhat suprisingly, forecasts made with the older NMC Limited Fine Mesh Model (LFM) were more reasonable. Next the importance of frontogenetical forcing and symmetric instability is assessed in conjunction with the US megalopolitan snowstorm of 11-12 February 1983 from Sanders and Bosart (1985a). A related large amplitude gravity wave is reviewed and extended to a similar case in February 1984. Finally, coastal frontogenesis is discussed in conjunction with the synoptic scale cyclogenesis problem along the US Atlantic coast.

1. Introduction

Much has been written about the observational, theoretical and numerical aspects of mesometeorology in the last decade. This paper will concentrate on the linkage between synoptic and mesoscale circulations accompanying cyclogenesis. Material will be drawn from both prior and ongoing case studies with emphasis on observational work. A common theme will be that a knowledge of the synoptic scale configuration is crucial to the understanding and prediction of a variety of important mesoscale phenomena. The reader interested in a broad overview of the mesoscale research problem should consult some recent general references in the field. See, for example, the books by Atkinson (1981), Browning (1982) and Ray (1986).

2. Western Atlantic Cyclogenesis Event of 22-23 February 1987

Fig. 1 shows the 48h ECMWF sea-level pressure and 500 mb forecasts verifying 1200 GMT 23 February. The corresponding ECMWF verifying analyses appear in Fig. 2. The forecast is terrible with the predicted cyclone along the East Coast of the United States a mere caricature of reality. An equally poor 48 h forecast (not shown) was made by the operational US NMC Nested Grid Model (NGM). Both models erred in a strikingly similar fashion. Namely, they failed to phase in properly troughs in the northern and southern branch of the westerlies prior to explosive cyclogenesis. These forecasts, initialized from 1200 GMT 21 February, failed to advect the southern trough eastward fast

enough and with sufficient intensity to phase in with the northern trough. Each succeeding operational run of the NGM and ECMWF model improved the forecast, given a proper representation of the troughs in the initial analysis fields. All forecasts, however, were deficient in capturing the explosive nature of the cyclogenesis in the 12h ending 1200 GMT 23 February and keeping the storm close enough to shore.

Lai and Bosart (1987) have described a case in November of 1980 in which a major cyclogenesis forecast failure occurred when the operational US models failed to simulate the phasing of two separate troughs in the mid tropospheric westerlies. In the November 1980 case the US models failed to predict the development of the northern trough. Rather, the southern trough was overpredicted and the resulting surface cyclogenesis was forecast too far south and was too weak. (A similar problem plagued the operational ECMWF model at that time as judged from the analysis and forecast maps archived in the ECMWF library). Lai and Bosart (1987) diagnosed the operational LFM 12 h forecast and analysis fields for the November 1980 case. They found that the LFM was unable to simulate properly the production of low level vorticity by convergence and its upward advection in ascent regions ahead of the deepening northern trough. As the two troughs phased in with the northern trough intensifying there appeared to be important non-linear interactions in progress. Lai and Bosart (1987) also indicated that the Rocky Mountain barrier may have played some not as yet understood role in the outcome of the cyclogenesis.

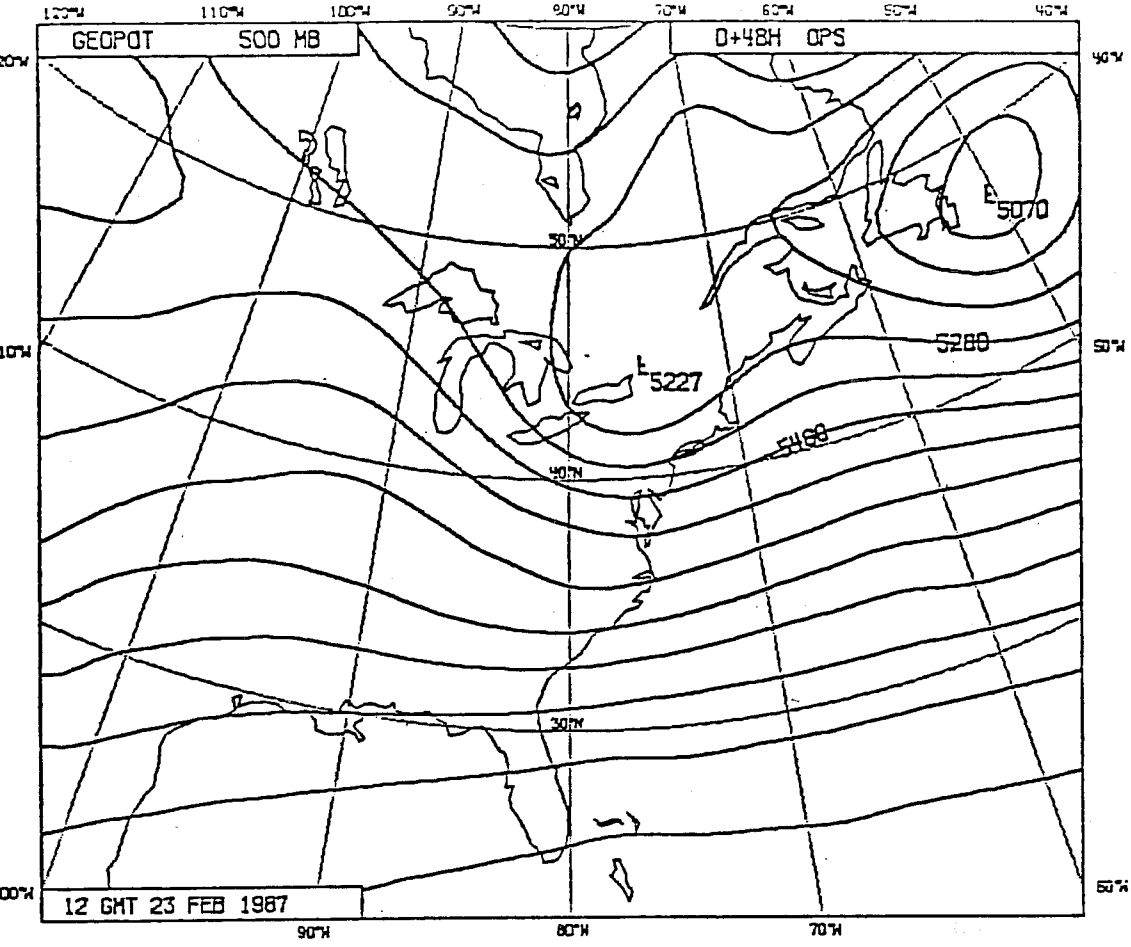

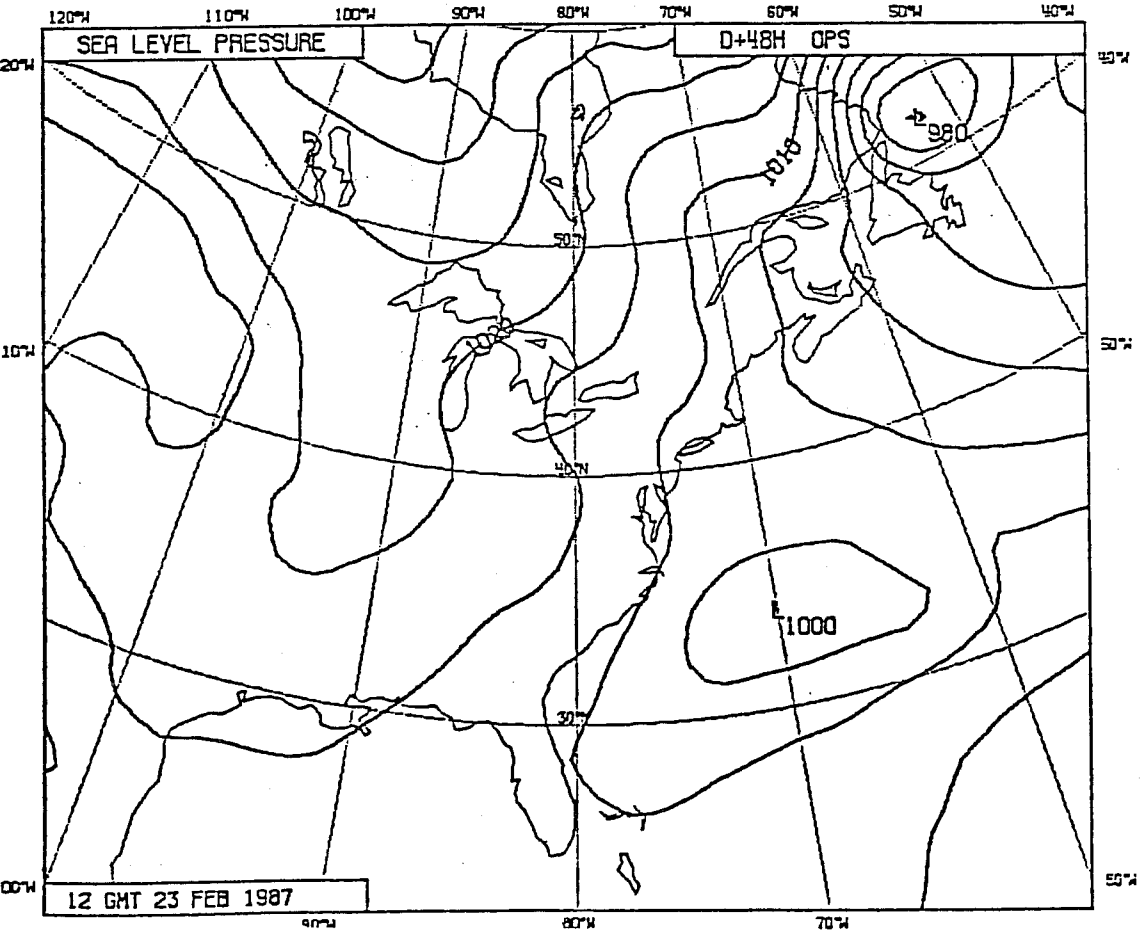

Fig. 1 ECMWF 48h 500 mb forecast (top) and mean sea-level pressure forecast (bottom) verifying 1200 GMT 23 February 1987.

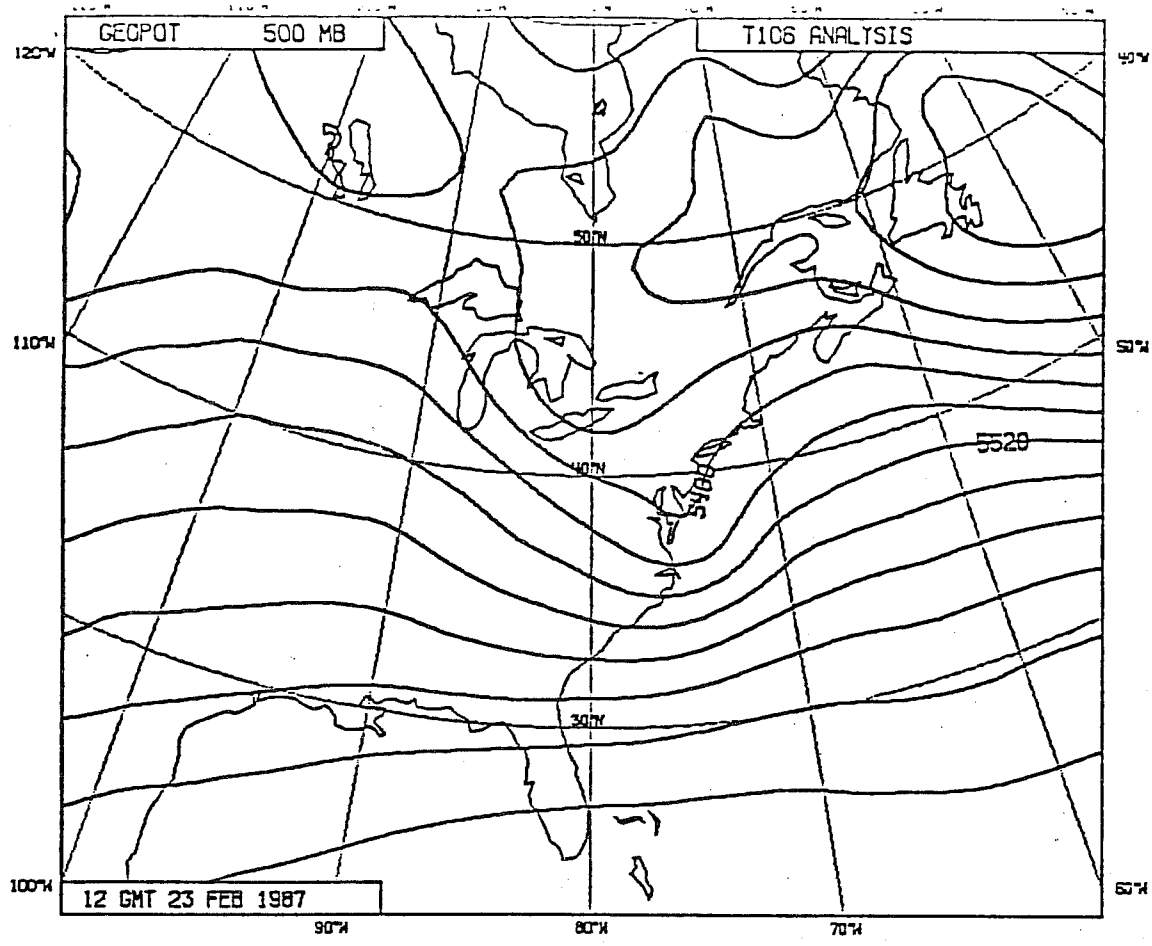

Fig. 2 As in Fig. 1 except for ECMWF verifying analyses.

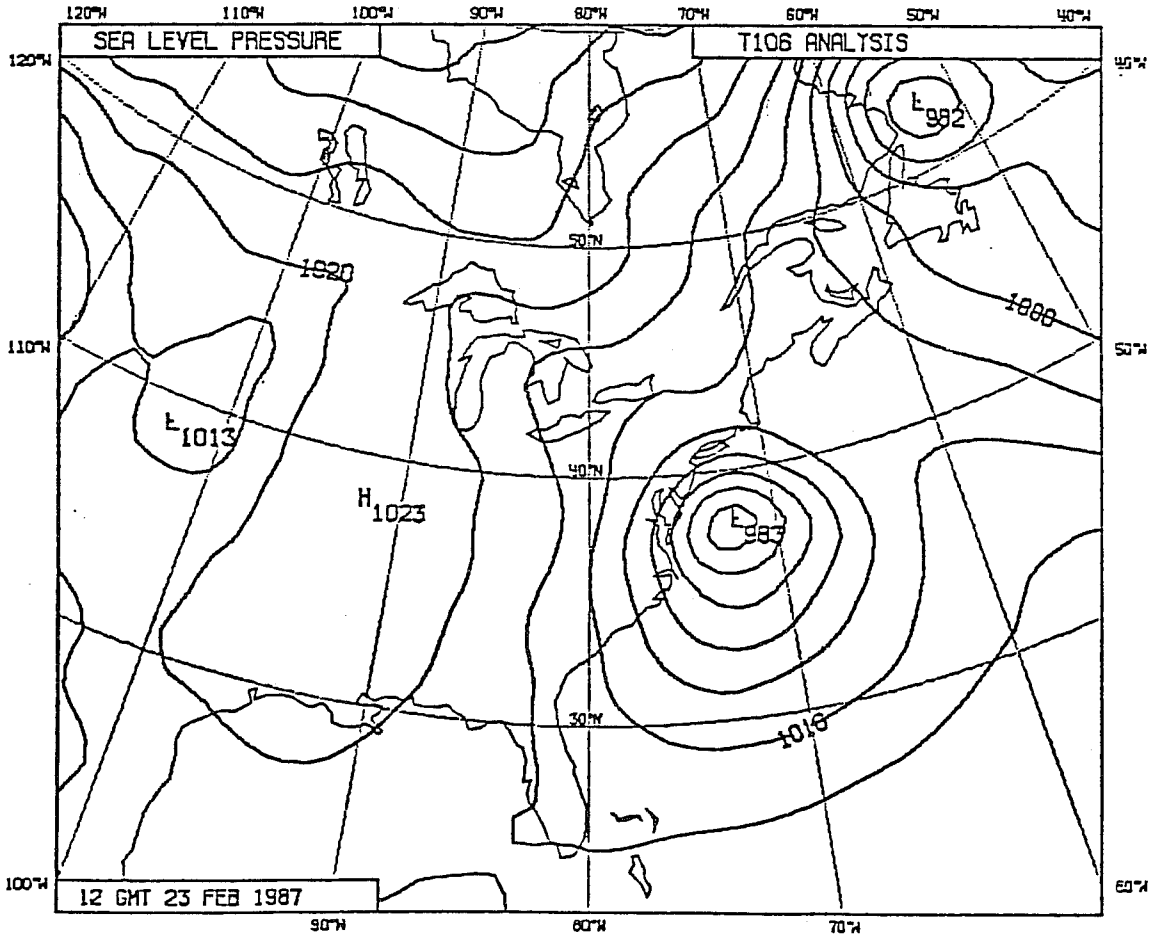

Several groups on both sides of the Atlantic have agreed to pool their research efforts on diagnostic and prognostic studies of the February 1987 storm. An additional motivation for the research is that the operational US LFM model, while not perfect, outperformed both the NGM and ECMWF models for all forecast projections. It seems crucial to understand why a simpler model with a more restricted data base should produce operationally more useful forecasts than the more sophisticated models.

An intriguing aspect of the February 1987 storm was that convection broke out near the storm center at the onset of explosive deepening. Figures 3 and 4 show the location of cloud to ground lightning strikes for the 0600-0900 GMT and 0900-1500 GMT 23 February periods respectively. The lightning flashes were recorded by the State University of New York at Albany (SUNYA) lightning location system (Orville et al., 1983). The plus signs indicate that positive charge was lowered to ground in many of the flashes near the rapidly deepening storm center just east of the Virginia - North Carolina coast. Experience with the SUNYA lightning network suggests that positive flashes are often associated with shallower convective cloud elements whose tops may be found in the 500-300mb layer.

Tracton (1973) noted that the operational NMC prediction models often failed to simulate the rate and intensity of cyclogenesis when convection was apparent near the incipient storm center. He hypothesized that the bulk effects of cumulus convection, not properly treated in the NMC models, contributed to the rapidity and intensity of cyclogenesis. The possible role

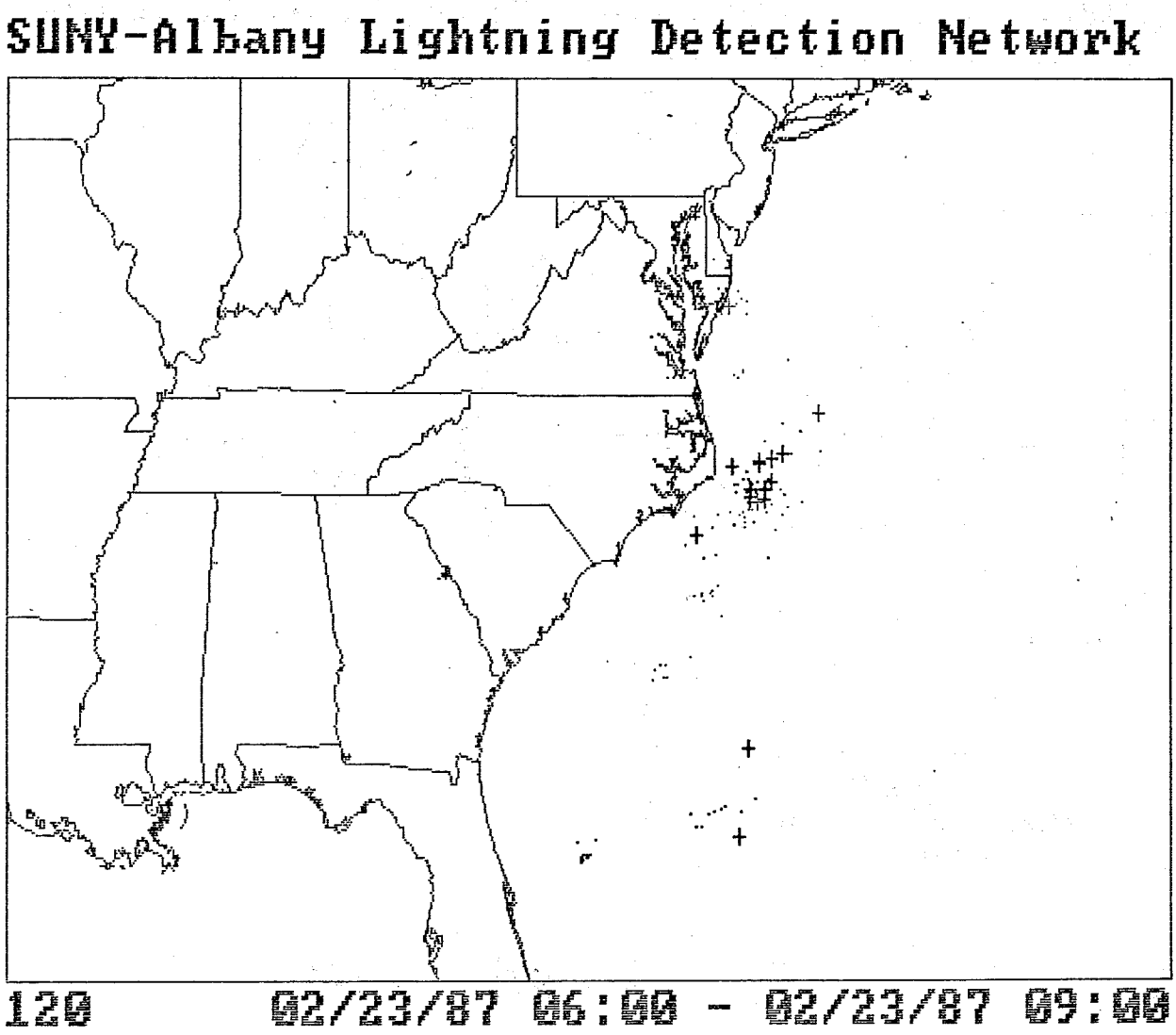

Fig. 3 State University of New York at Albany (SUNYA) cloud to ground lightning flash locations for the three hour period ending 0900 GMT 23 February 1987. Plus (dots) signs indicated positive (negative) charge lowered to ground.

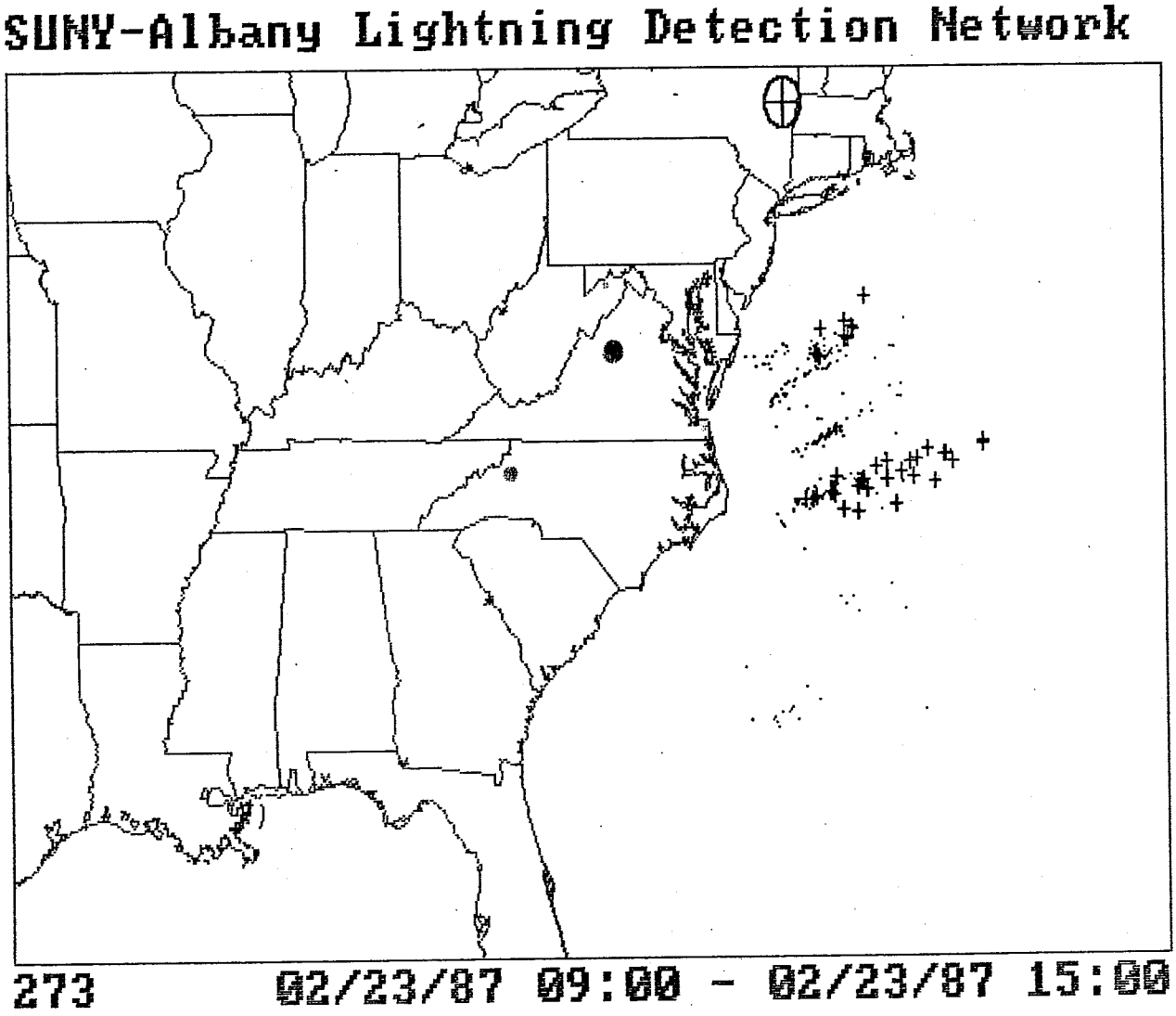

Fig. 4 As is Fig. 3 except for the six-hour period ending 1500 GMT 23 February 1987.

of convection versus baroclinic processess in the cyclogenesis process has been debated in the open literature for polar lows (Reed, 1979; Rasmussen, 1985 and Shapiro et. al., 1987) and explosive oceanic cyclones (Gyakum, 1983 a, b; Uccellini, 1986; Anthes et al., 1983; Bosart, 1981; Bosart and Lin, 1984; Uccellini et al., 1984, 1985 and Reed and Albright 1986). A question that can be posed is to what extent the explosive deepening phase of a cyclone can be viewed as a mesoscale process. The existence of relatively shallow convective elements in the storm environment may be an important clue, however, in that the level of maximum heating is lower in the troposphere (700 mb). Storm spin-up would be enhanced when horizontal convergence is concentrated in the lower troposphere as noted by Bosart (1981). Hopefully, it will be possible to report progress on understanding the nature of the February 1987 cyclogenesis event in future seminars and papers.

3. Megalopolitan Snowstorm of 11-12 February 1983

Frontogenetical forcing and symmetric instability may play an important role in some cyclogenesis events. One such case was the major Atlantic coast storm of 11-12 February 1983. Excerpts from Sanders and Bosart (1985a) are used to describe the storm here.

3.1 Preliminaries

An intensifying cyclone moved northeastward from the vicinity of Cape Hatteras during 11-12 February 1983, the center passing some 300 km offshore from the south coast of New England. The synoptic situation is illustrated in Fig. 5. The storm produced

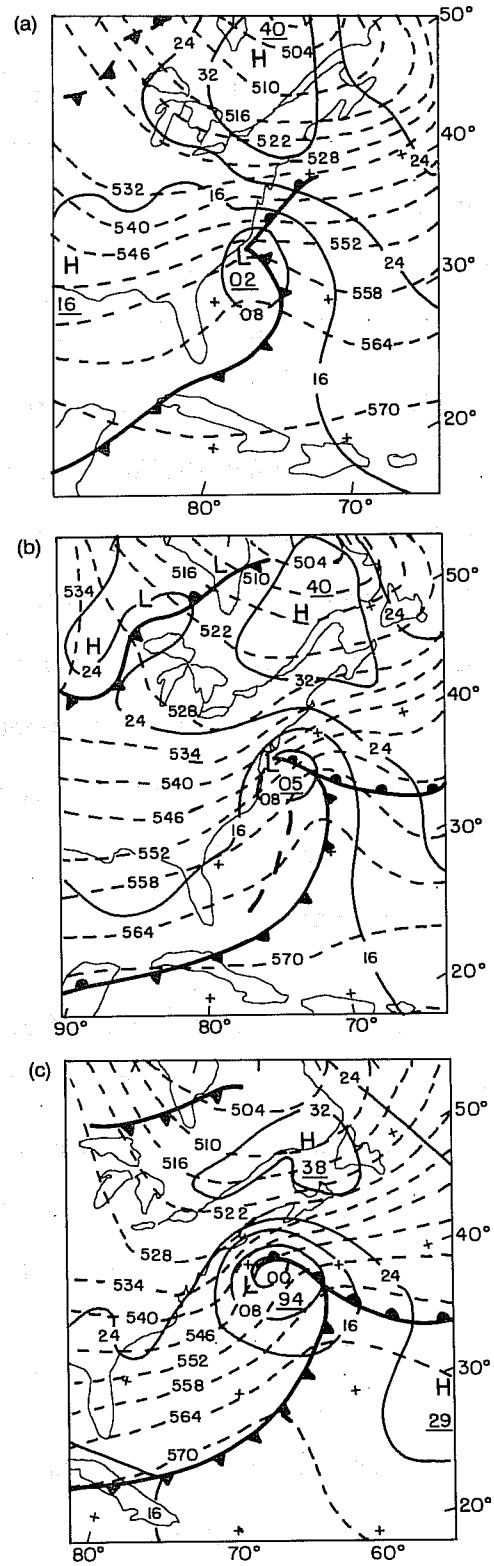

FIG. 5. Sea level isobars (solid lines, at intervals of 8 mb) and pressure centers, surface fronts (conventional notation) and thickness of the layer from 1000 to 500 mb (dashed lines, at intervals of 6 dam) for (a) 1200 GMT 11 February; (b) 0000 GMT 12 February; (c) 1200 GMT 12 February.

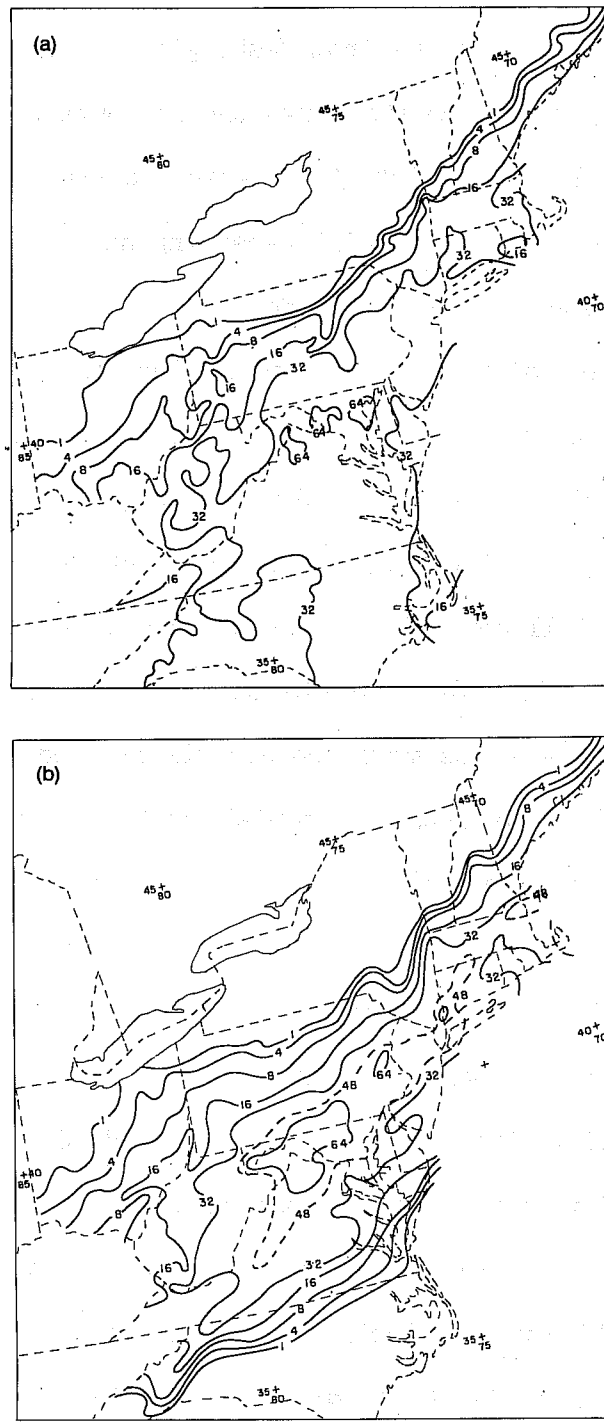

FIG. 6. Total precipitation 10–12 February 1983: (a) total rain and/or equivalent liquid depth of frozen precipitation (mm); (b) depth of snowfall (cm).

abundant precipitation (Fig. 6), with a band of heavy snow from western North Carolina northeastward across or near every large city in the megalopolis extending from Washington to Boston.

An important aspect of the storm was the narrowness of the band of heavy snow. Its half-width (the lateral distance from the point of maximum fall to the point receiving half this amount) ranged from about 50 km in the North Carolina mountains to about 125 km in central Virginia to about 75 km in New England. These distances are clearly in the mesoscale range. In the southwest the distribution was no doubt strongly conditioned by orography. In Virginia and Maryland substantial amounts of ice pellets and rain fell southeast of the region of maximum snow depth, as seen in Fig. 6a. Thus the total precipitation produced by the storm here was more broadly distributed. It is still seen that the locus of maximum snowfall and maximum precipitation were nearly coincident. In New England the precipitation was entirely in the form of snow in an unusually intense band lying at a typical distance northwest of the surface cyclone center (Brooks and Schell, 1950). We will here present evidence, derived mainly from analysis of rawinsonde data, that the concentration of precipitation was a manifestation of frontogenetical forcing within or adjacent to a region of small moist symmetric stability. Instability of this type may have occurred as well. A more detailed study of the situation in New England, based mainly on analysis of Doppler radar observations appears in Sanders and Bosart (1985b). An investigation of an intense singular gravity wave, accompanied by thunderstorm

activity as it propagated northeastward is presented in Bosart and Sanders (1986).

3.2 Physical Mechanisms

The band of heavy snow was oriented approximately along the thermal wind (cf., Fig. 5). Such banded structure is a pervasive feature of cyclone-scale precipitation areas. Heymsfield (1979), Herzegh and Hobbs (1980) and Houze et al. (1981) have studied warm-front cases somewhat similar to the present one, but have addressed mainly the cloud-microphysical aspects. Two dynamical mechanisms that might be responsible for this phenomenon are frontogenetical forcing and symmetric instability.

The former was first empirically described ty Bjerknes (1919) in terms of ascent of warm air over a wedge of cold air. Subsequent work by Namias and Clapp (1949), Sawyer (1956), Eliassen (1959) and Hoskins and Bretherton (1972) has shown in physical terms how ascent of warm air and descent of cold air occurs. With large-scale geostrophic confluence acting to increase the horizontal temperature gradient by horizontal advection and to decrease the vertical wind shear by horizontal momentum advection, thermal-wind balance is upset. A thermally direct transverse circulation is induced to restore this balance, as sketched in Fig. 7a. The warm ascent is broad and gentle, and a discontinuity develops only at a boundary. Recent work by Emanuel (1985) and Thorpe and Emanuel (1985), however, shows that if the potential vorticity vanishes in the warm air, then the ascent may become intense and concentrated, as shown in Fig. 7b. Qualitatively, in this case the gravitational and

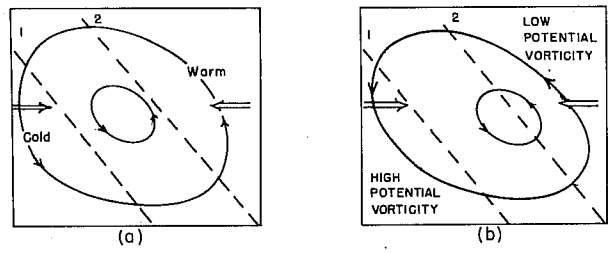

Fig. 7. Vertical cross sections of idealized transverse circulations accompanying large-scale frontogenetical confluence (double-shafted arrows): (a) uniform potential vorticity and (b) vanishing potential vorticity in warmer air. Dashed lines are potential isotherms.

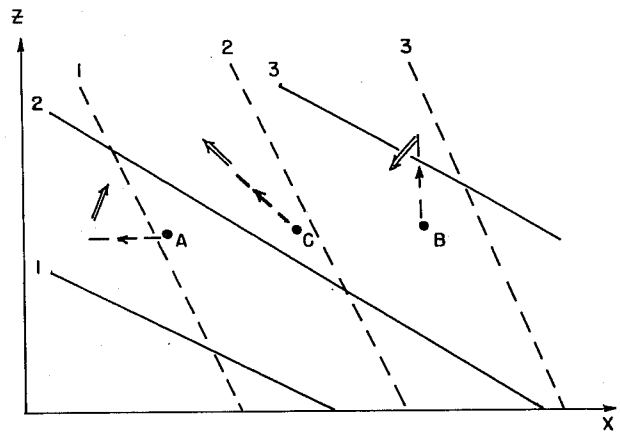

FIG. 8. Schematic vertical cross section illustrating symmetric instability. Solid lines represent absolute momentum $\bar{M}$ of basic flow. Dashed lines represent equivalent potential temperature. Lettered points show sample displacements (dashed) and accelerations (arrowheads). See text.

inertial resistance to sloping ascent vanishes, so that the updraft is relatively vigorous for a given frontogenetical forcing. The downdraft is not enhanced and since upward and downward mass fluxes must still balance, the updraft must be also horizontally restricted, producing the possibility of a mesoscale band of precipitation.

As to the latter mechanism, Bennetts and Hoskins (1979) and Emanuel (1979) have suggested symmetric instability in saturated air as an explanation for band organization. Emanuel (1983a,b) has recently elaborated on the theory and measurement of some integral properties of this phenomenon, which we might refer to as "slantwise convection."

A schematic vertical cross-section normal to a geostrophically balanced base-state flow, with vertical shear in the direction of the flow, appears in Fig. 8. The speed of this flow, $\bar{v}$, is chosen to increase with elevation and to be independent of x, the horizontal direction in the plane of the section. The air is everywhere saturated. Following Emanuel (1983a), we show the distribution of $\bar{M} \equiv \bar{v} + fx$ increasing to the right (since f is taken positive) and increasing upward. Since there is no horizontal pressure-gradient force in the y-direction and since we take no account of viscous effects, $\bar{M} \equiv \bar{v} + fx$ is conserved for an individual displaced parcel (or perhaps better a displaced tube extending indefinitely in the y-direction). We choose a stratification in which the equivalent potential temperature of the base state θ_e increases upward. We assume thermal wind balance. Thus θ_e increases to the right since, following Emanuel

(1983a) and Durran and Klemp (1982)

$$\frac{\partial \bar{w}}{\partial z} = \frac{g}{\mp} \frac{\Gamma_m}{\Gamma_d} \frac{\partial \ln \bar{\theta}_e}{\partial x} \qquad (1)$$

where Γ_m and Γ_d are saturated- and dry-adiabatic lapse rates. Since we assume moist-adiabatic themodynamics, θ_e is conserved for a displaced parcel

Accelerations for a displaced parcel in the x-and z-directions in this case (neglecting the effects of pressure perturbations associated with the displacement) are, respectively,

$$\frac{du}{dt} = \mp \left[M - \bar{M} \right] \equiv \mp M' \qquad (2)$$

$$\frac{dw}{dt} = g \left[\frac{\theta - \bar{\theta}}{\bar{\theta}} \right] \equiv \frac{g\theta'}{\theta} = g \left[\frac{\theta_e'}{\bar{\theta}_e} - (\exp Q' - 1) \right] \qquad (3)$$

where $Q' \equiv Lq'/C_pT$. (For practical purposes $\theta' \approx \theta'_e/2$ for much of the observed range of saturated atmospheric conditions in the middle troposphere. It approaches 0.2 in warm air near the surface and unity in cold upper-tropospheric conditions.) It is readily seen from Fig. 8 that purely horizontal or vertical displacements, shown schematically by points A and B, are stable. For point A, for example, a leftward horizontal displacement produces an excess of parcel M over background $\bar{M}$. Hence $M' > 0$ and from (2) $du/dt > 0$. That is, the horizontal acceleration is to the right, so as to restore the parcel to its initial position. In this case the displayed parcel is positively buoyant, since $\theta_e > \bar{\theta}_e$. The resulting upward acceleration, however, does not mitigate the horizontal acceleration back to the point of origin and does not continue as the thermal stratification is stable;

$\partial\bar{\theta}_e/\partial z > 0$. Analogous consideration of the case of vertical displacement, illustrated by point B, also shows stability. For the displaced parcel, $\theta_e < \bar{\theta}_e$ so that the resulting vertical component of acceleration is downward, toward the level of origin. In this case $M < \bar{M}$ for the displaced parcel; thus $M' < 0$ and $du/dt < 0$. However, this horizontal acceleration does not affect the stable downward vertical acceleration and quickly lessens because the momentum structure is inertially stable; $\partial\bar{M}/\partial x > 0$.

Note, however, that the slantwise displacement for point C, with slope intermediate between those of the $\bar{M}$- and $\bar{\theta}_e$-isopleths, is unstable, i.e., M' and θ'_e have the same sign as the x- and z-components of the displacement, so that the resulting acceleration has a component in the direction of the displacement. It can be seen that slantwise instability requires the slopes of the $\bar{M}$-surfaces to be shallower than those of the $\bar{\theta}_e$-surfaces. From elementary geometrical considerations, the slope of an M-surface in the z-x plane can be expressed by

$$\left(\frac{\delta z}{\delta x}\right)_{\bar{M}} = \frac{-\partial\bar{M}/\partial x}{\partial\bar{M}/\partial z}$$

From the definition of $\bar{M}$, this slope is given by

$$\left(\frac{\delta z}{\delta x}\right)_{\bar{M}} = -f + \frac{\partial\bar{u}/\partial x}{\partial\bar{u}/\partial z}$$

Similarly, the slope of a $\bar{\theta}_e$-surface can be expressed by

$$\left(\frac{\delta z}{\delta x}\right)_{\bar{\theta}_e} = \frac{-\partial\bar{\theta}_e/\partial x}{\partial\bar{\theta}_e/\partial z}$$

From the thermal-wind relationship (1) this latter slope can also be expressed as $\left(\frac{\delta z}{\delta x}\right)_{\bar{\theta}_e} = -\left(\frac{\bar{\theta}_e}{g}\right)\left(\frac{\Gamma_d}{\Gamma_m}\right) + \frac{\partial\bar{v}/\partial z}{\partial\bar{\theta}_e/\partial z}$

The condition that the $\bar{M}$-surfaces be shallower than the

$\bar{\theta}_e$-surfaces is that

$$\frac{(\delta z/\delta x)_{\bar{M}}}{(\delta z/\delta x)_{\bar{\theta}_e}} = \left(\frac{\bar{\eta}}{f}\right)\left(\frac{\Gamma_m}{\Gamma_d}\right)\frac{g}{\bar{\theta}_e}\frac{(\partial\bar{\theta}_e/\partial z)}{(\partial\bar{v}/\partial z)^2} \equiv Ri_{sc} < 1$$

where $\bar{\eta} = f + \frac{\partial \bar{v}}{\partial x}$ is taken as the absolute vorticity and Ri_{sc} has been introduced because it seems reasonable to refer to the ratio as the "Richardson Number for slantwise convection." Another way of viewing the criterion for instability is obtained by noting that if the slope of the $\bar{M}$-surfaces is shallower, with $\bar{M}$ increasing upward, then $\bar{M}$ decreases in the positive x-direction along a $\bar{\theta}_e$-surface. From the definition of $\bar{M}$, this is equivalent to stating that

$$\left(\frac{\partial \bar{v}}{\partial x} + f\right)_{\bar{\theta}_e} = \bar{\eta}_{\bar{\theta}_e} < 0$$

The importance of negative absolute vorticity along $\bar{\theta}_e$-surfaces in the stimulation of inertial motions was discussed by Bjerknes (1951), but in the context of an amplifying synoptic-scale circulation rather than smaller-scale instability.

Finally, we should note that the coefficient, $g/\bar{\theta}$, in (3) is about 300 times larger than the middle-latitude coefficient f in (2). Therefore, unless θ', and thus θ'_e, are extremely small the vertical acceleration will utterly dominate the horizontal one. Equivalently, the motions will tend to be nearly along the $\bar{\theta}_e$ surfaces.

3.3 Measurements of frontogenetical forcing and evidence for Symmetric instability

The gross structure of the troposphere north of the surface cyclone at an early stage of the storm's impact upon megalopolis is illustrated in Fig. 9. The flow was broadly frontogenetical,

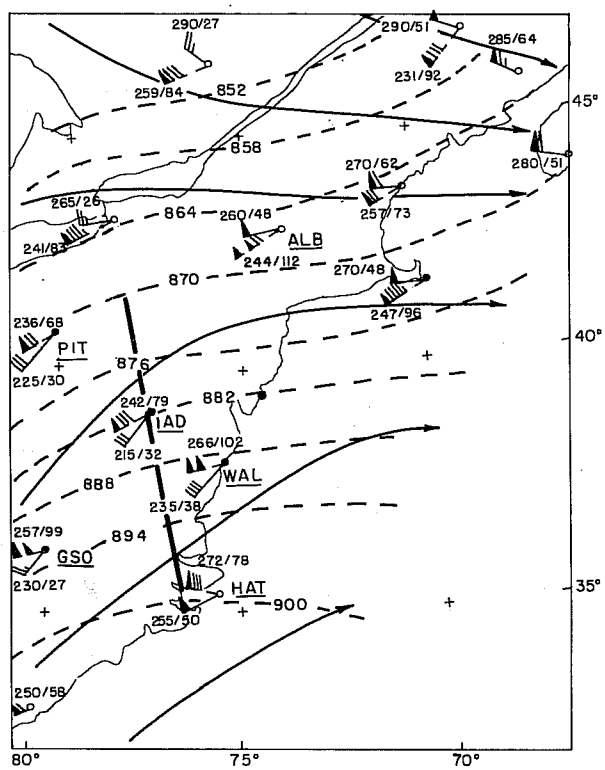

FIG. 9 Contours at 500 mb (solid lines, at intervals of 6 dam) and thickness of the layer from 850 to 250 mb (dashed lines, at intervals of 6 dam). Plotted winds for 500 mb (solid shaft) and for shear from 850 to 250 mb (dashed shaft). Each pennant, full barb and half barb corresponds to 25, 5 and 2.5 m s^{-1}, respectively. (Plotted numbers denote direction in degrees and speeds in knots.) Filled station circles indicate dew-point depression less than 5°C. Heavy line shows position of cross section in Fig. 10. For 1200 GMT 11 February.

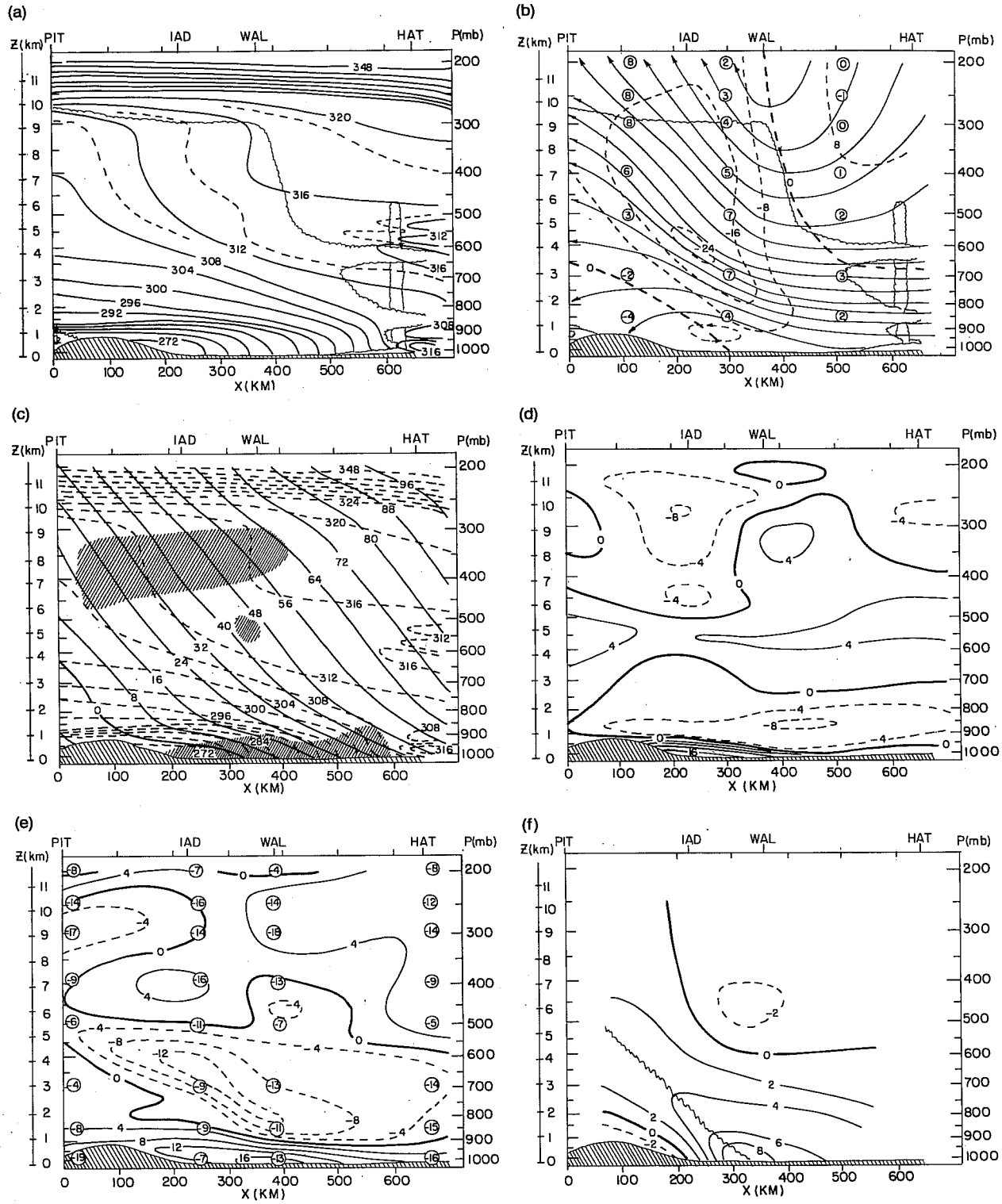

FIG. 10. Vertical cross sections PIT–HAT, 1200 GMT 11 February 1983. (a) Equivalent-potential temperature at intervals of 4 K, with schematic cloud mass indicated by scalloped line. (b) Streamfunction ψ^x (solid lines, at intervals of 8×10^2 mb m s^{-1}) and vertical motion, ω^x (dashed lines at intervals of 8×10^{-3} mb s^{-1}). Circled numbers are estimates of ω^y. See text. Cloud outline added. (c) Absolute geostrophic momentum M_g (solid lines, at intervals of 8 m s^{-1}) and equivalent-potential temperature (dashed), as in (a). Shading denotes areas of symmetric instability. (d) Ageostrophic v-component (m s^{-1}, from 255°). (e) Ageostrophic u-component (m s^{-1}, from 345°). Circled numbers are geostrophic u-components. (f) Geostrophic frontogenesis, $-(\partial u_g/\partial x)(\partial T/\partial x)$, at intervals of 2×10^{-5} K (100 km)$^{-1}$ s^{-1}. Jagged line shows axis of maximum frontogenesis.

since there was warm advection everywhere south of the 876-decameter (dam) thickness line and cold advection north of the adjacent 870-isopleth. Winds at 500 mb and wind shears over the layer were not far from geostrophic balance except at ALB, where the data were extrapolated from a sounding that failed below the 250 mb level and may have been wrong. Within the layer, however, we shall find a prominent ageostrophic circulation.

To illustrate the structure in more detail, we projected the soundings from PIT, IAD, WAL and HAT on the cross-section line shown in Fig. 9 oriented 345-165°, normal to the thermal wind in the layer from 850 to 250 mb. Analyses of the field of equivalent-potential temperature θ_e and of the estimated area of saturation (derived from rawinsonde humidities, surface observations and satellite imagery) appear in Fig. 10a. Except at HAT the vertical structure of the θ_e-field shows four layers: a reasonable well-mixed surface boundary layer 75 to 100 mb deep, a stable layer extending upward to the middle troposphere, a layer with small conditional stability occupying the middle to upper troposphere, and the stable stratosphere above a tropopause between 250 and 300 mb. The air was at, or close to, saturation throughout and snow was observed at the ground, with moderate intensity at IAD. At HAT a more complicated structure was observed, with a number of relatively thin layers of saturated air and with potential instability for parcels originating in the thin stratum of high θ_e just above an ocean-cooled surface layer. The schematic cumulus cloud is based on this instability and on the observation of occasional moderate rain at HAT at 1100 GMT.

The edge of the deep cloud between WAL and HAT is estimated from satellite IR imagery.

The motion in the plane of the section is approximated by the mass streamfuction Ψ^x shown in Fig. 10b. It is defined by

$$\Psi^x(p) \equiv \int_p^{p_s} u\,dp$$

where p_s is pressure at the surface and u is the wind component from 345°. The x-axis is taken toward the right in the plane of the section, for consistency with Fig. 8. The Ψ^x-field represents u exactly.

As for the vertical motion, consider the equation of continuity of mass in a cartesian frame

$$\omega(p) \equiv \frac{dp}{dt} = \int_p^{p_s} \left(\frac{\partial u}{\partial x} + \frac{\partial v}{\partial y}\right) dp = \frac{\partial \Psi^x}{\partial x} + \frac{\partial \Psi^y}{\partial y} = \omega^x + \omega^y$$

where

$$\Psi^y \equiv \int_p^{p_s} v\,dp \;;\quad \omega^x \equiv \frac{\partial \Psi^x}{\partial x} \;;\quad \omega^y \equiv \frac{\partial \Psi^y}{\partial y}$$

In the present case, owing to the elongation of the precipitation area from east-northeast to west-southwest, and to the previously mentioned frontogenetical character of the synoptic-scale flow, we assume that ω^x, which can be obtained from the streamfunction field shown in Fig. 10b, is larger than ω^y and represents the total vertical-motion field reasonably well, at least in the lower and middle troposphere. This picture will exaggerate the ascent, since with the confluent flow, $\partial v/\partial y > 0$. An estimate of ω^y can be obtained by assuming that $\partial v/\partial y$ is approximately given by $-\partial u_g/\partial x$, u_g being the geostrophic value to be obtained later for another purpose. Resulting values of ω^y at selected points are also shown in Fig. 10b.

In this diagram, ω^x shows a strong sloping updraft along the transition zone at the base of the layer of small conditional stability. Its horizontal half-width was about 100 km. Maximum ascent was found in the middle and upper troposphere near IAD, where the heaviest snowfall was observed at this time. At 200 mb, in the lower stratosphere where the vertical motion should be slight, the correction produced by ω^y removes most of the ascent from ω^x. This correction reduces the maximum ascent near 600 mb level by about 20%. (The corrected kinematical vertical motion is between 20 and 30 cm s^{-1} in the major updraft on 100 km scale between the 700 and 300 mb levels.) The descent above 600 mb over and northwest of HAT corresponds to a region of very dry air above 550 mb observed there. The correction fails to remove the pronounced descent at 200 mb, which must be regarded as spurious, possibly owing to unreliability of the geopotential analysis over the ocean, from which the correction was derived.

For assessment of the possibility of symmetric instability, Fig. 10c combines the fields of θ_e and $M_g \cong v_g + fx$. The latter quantity was calculated by multiplying $f(9 \times 10^{-5}\ s^{-1})$ by the distance along the section to the right of PIT and adding v_g, the component of geostrophic wind into the plane of the section, measured by differencing the geopotential over distances of about 200 km along the section from a series of analyses at standard pressure levels. In the context of the preceding section, M_g is identified with $\bar{M}$. The geostrophic value must be used because $\bar{M}$ contains a representation of the horizontal pressure-gradient

force through $\bar{v}$, which is assumed to be in geostrophic balance. We see in Fig. 10c a region of slantwise instability in the region of small hydrostatic stability in the upper troposphere between PIT and WAL. An extension of small or negative slantwise stability to lower levels is seen at WAL. This region is downwind in the large scale flow from a region of modest latent instability for upright convection, as documented by the soundings at HAT and at GSO (not shown). If we visualize a trajectory in the large scale flow, perhaps ordinary convection occurs first, removing the irregularities in the θ_e-profile and leaving a nearly neutral stratification with sufficient vertical wind shear to make the structure symmetrically unstable. A third region where the M_g-isopleths are shallower than the θ_e-isotherms is the lowest kilometer over most of the section. Our inviscid mechanism, however, does not seem applicable to this region, where the surface viscous force is surely important. It is noteworthy that thunderstorm activity described by Bosart and Sanders (1986) broke out not far from IAD, in a region where there was no evidence of buoyancy for conventional upright convection, but where a deep atmospheric layer displayed slight or negative symmetric stability.

The practical application of (4) to individual soundings requires association of the vertical shear of the observed wind with the shear of the geostrophic wind. The reliability of this association can be gauged by an examination of the ageostrophic v-components, which are shown in Fig. 10d. The largest values are within or immediately adjacent to the surface boundary layer.

Above this, a patchy pattern with maximum magnitudes near 4 m s^{-1} probably represents errors in the observations or analysis and small-scale variability not adequately resolvable in the routine data. These results constitute a warning that shallow layers of observed wind shear indicating slantwise instability should be regarded with caution.

The applicability of the idealized section in Fig. 8 must be questioned because the basic flow was not in the same direction as the thermal wind, as seen for example in Fig. 9. The conservation of M is based on the premise of no force, or more generally no net force in the y-direction. If the u-components of motion are not in geostrophic balance then there is a net force in the y-direction. Hence it is desirable to estimate the ageostrophic u-components. They appear in Fig. 10e, displaying a prominent circulation below 500 mb, positive (from cold to warm) in potentially cold air near the ground and negative (from warm to cold) in potentially warmer air above. Maximum magnitudes were in excess of 12 m s^{-1} and the dividing line sloped upward toward the northwest, from 940 mb near HAT to 700 mb between IAD and PIT. This circulation constituted the horizontal limb of the vigorous pattern of ascent shown in Fig. 10b. Above 500 mb a patchy cellular pattern is seen, with maximum values near 4 m s^{-1}. Little significance is attached to this pattern. In much of this upper region, then, the force in the y-direction was relatively small, and the finding of low symmetric stability seems defensible.

There is a clear indication in Fig. 10b of an intense

transverse frontal circulation below 500 mb. Moreover, the geostrophic u-components, appearing in Fig. 10e, showed pronounced lower-tropospheric confluence. We calculated the geostrophic frontogenetical forcing $-\left(\frac{\partial u_g}{\partial x}\right)\left(\frac{\partial T}{\partial x}\right)$ from

$$-\frac{\partial u_g}{\partial x}\frac{\partial T}{\partial x} = \frac{Pf}{Q}\frac{\delta u_g}{\delta x}\frac{\delta w_g}{\delta p}$$

where δx and δp were taken as 200 km and 100 mb, respectively. The results appear in Fig. 10f. There was a broad zone of frontogenesis with central intensity of several ^{o}C $(100\ km)^{-1}$ per day. Maximum strength was at the ground near WAL, extending upward and northwestward to the 500 mb level between PIT and IAD. Frontolytical forcing occurred above 600 mb southeast of IAD.

Comparing Figs. 10e and f, we see that the axis of maximum geostrophic frontogenesis lay near the maximum positive ageostrophic u at the ground but extended up into negative values above 800 mb. Maximum negative ageostrophic u occurred about 100 km from the axis of frontogenesis, toward the warmer air. Comparing Figs. 10b, and f, we see that maximum ascent occurred in a band nearly parallel to the axis of frontogenesis, being displaced horizontally about 100 km from, it, toward the warmer air, and about 200 mb (2.5 km) above it. This structure strongly resembles a recent theoretical result of Emanuel (1985), from a diagnostic semigeostrophic model with a discontinuity in potential vorticity. The discontinuity is along a line parallel to, and some distance toward the warmer air from, the axis of maximum frontogenesis. Positive values below this line drop to zero above it. In the present case, the region of small

potential vorticity(cf. Fig. 10c) lies above the frontogenetical axis, consistent with the model structure.

We conclude that at this time the intense updraft seen over IAD in Fig. 10b was a concentrated response to large-scale frontogenetical forcing. The intensity and size in the mesoscale range is attributable to low symmetric stability in the warmer air, while symmetric instability per se may have produced structure in the upper portion of the cloud system without having a large effect upon precipitation at the surface.

4. Large amplitude gravity waves

Uccellini and Koch (1987) have recently examined the synoptic setting of 13 cases of mesoscale wave disturbances known more commonly as gravity waves. The waves themselves may be characterized by wave packets or a singular wave of depression with periods of 1-4h, horizontal wavelengths of 50-500 km and surface pressure perturbations of 0.5-7.0 mb. The typical synoptic setting finds the wave located north of a quasi-stationary surface frontal zone in the presence of a pronounced thermal inversion in the lower troposphere. Aloft a significant jet streak exit region lies upstream in the advancing trough with a jet entrance region found downstream toward the ridge axis. Many of the cases appear to satisfy the Lindzen and Tung (1976) criteria for the maintenance of ducted gravity waves. Uccellini and Koch (1987) argue that geostrophic adjustment in the exit region of the advancing jet streak might be the major source mechanism for most of their wave cases. They do not rule out shearing instability and convection as wave sources although

they argue that the lack of a correlation between wave amplitude and the existence of convection weakens arguments for convection as a dominant wave source.

The megalopolitan snowstorm of 11-12 February 1983 featured a long-lived large amplitude gravity wave that broadly satisfied the synoptic patterns described by Uccellini and Koch (1987). Excerpts from Bosart and Sanders' (1986) description of the storm follow.

A striking aspect of the storm was a line of hourly-scale pressure oscillations of large amplitude, oriented approximately normal to the thermal wind. The singular perturbation was similar in strength and longevity to pulses described by Brunk (1949), Pothecary (1954), Wagner (1962), Ferguson (1967), Bosart and Cussen (1973), Eom (1975) and Pecnick and Young (1984). Like these examples, it displayed the character of a gravity wave. Unlike them, it was embedded in a region of continuous heavy precipitation and was directly associated with thunderstorms during its period of peak strength.

Some quantitative characteristics of the presssure oscillation and of the accompanying electrical activity are displayed in an illuminating manner in Fig. 11. The double amplitude, $2(\Delta p)'$, of the wave containing the leading fall center (A) was estimated by subtracting the greatest observed one-hour fall from the average of the two nearest maximum rises at stations (or minimum falls) along a general southwest-northeast direction. Similarly for the rise center (B), with maximum and minimum reversed of course, and for the trailing fall

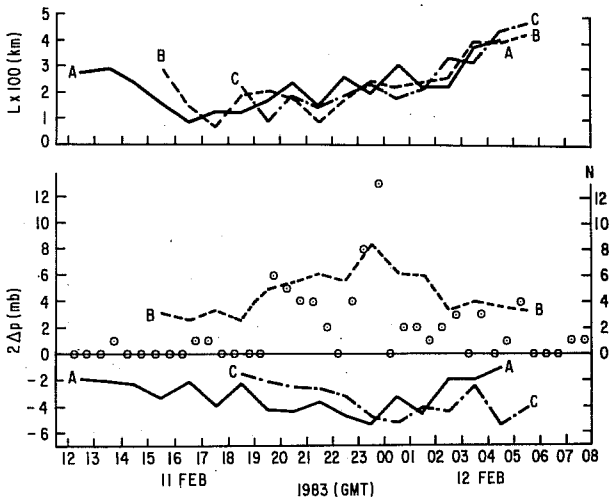

FIG. 11.-Time series of the wave length, L (top), and the double amplitude, $2(\Delta p)'$ (bottom), for the region B centered on the rises (dashed lines) and of the regions A (solid lines) and C (dash-dot lines) centered on the leading and trailing falls, respectively. See text. The circled dots indicate the number of lightning flashes detected by the SUNYA system each half-hour.

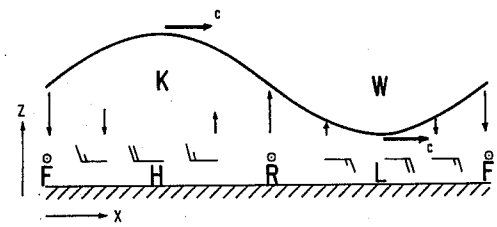

FIG. 12.Idealized vertical cross section of a linear plane gravity wave, with no basic current, propagating toward the right at speed, c. The heavy sinusoidal line is a representative isentropic surface or a temperature inversion. Surface pressure extrema are labeled H and L, while cold and warm temperature anomalies are denoted K and W, respectively.

center (C). The wave length, L, was taken as the distance between the locations of the two flanking extremes. Small irregularities in the times series of $2(\Delta p)'$ and L arise from the necessity of using discrete station values. Lightning occurrences were counted within each half-hour period.

The first identification of the pressure waves shows a double amplitude of 2-3 mb h^{-1} and horizontal scale about 200 km. Since the falls A precede the rises B, and the two are of equal magnitude, the wave appears first as a "hole" in the atmosphere, as in some of the cases cited, notable that of Pecnick and Young (1984). The scale of the oscillation shrinks to about 100 km 2-4 h after initiation, then slowly grows to nearly 500 km by the end of the observation period 12 h later. The double amplitude of the rise increases markedly with the onset of electrical activity, the peak of the rises reaching 8 mb h^{-1} at the time of maximum strike frequency. The system then appears more like a typical "thunderstorm high." Then both subside, the rises more abruptly than the lightning. Meanwhile the flanking falls intensify more slowly to double amplitudes of almost 6 mb h^{-1}, C becoming more prominent than A after 00 GMT, as the residual electrical activity becomes associated with it.

Various measures of the velocity of the disturbance can be obtained once the pressure features have become unambiguously established. The rise center, for example, moves toward 050-060 deg, at 15 m s^{-1} between 16 and 00 GMT, then accelerates to 18 ms^{-1} between 15 and 21 GMT, accelerating to an average speed of 22 ms^{-1} over the next 5 h prior to losing its identity.

The trailing center moves at 17 m s^{-1} between 19 and 02 GMT before accelerating to 23 m s^{-1} from that time until 06 GMT. All three components of the system thus start out at a speed of about 15 ms^{-1} and accelerate to more than 20 m s^{-1} after a few hours.

4.1 Effects on weather elements

4.1a Wind

The influence of this gravity wave on the weather elements can be inferred from the idealized vertical cross section after Eom (1975), shown in Fig. 12. (The vector difference between the gravity wave phase velocity and the basic current determines the dynamics of gravity wave behavior. Omission of the basic current in the simple model shown in Fig. 12 is permissible here because the wave is propagating rapidly against the basic flow which allows for the rapid transit time of an individual air parcel through the gravity wave disturbance. For a gravity wave propagating slower than the basic current the attendant vertical motions, pressure falls and wind perturbations shown in Fig. 12 would be reversed). As the low-pressure trough approaches, in the model, the wind increases from the direction toward which the wave is propagating. In the present case, the wave is traveling toward the northeast, against a substantial northeasterly basic current, which must be added to the model. The northeasterly wind should therefore increase to maximum strength at the time of lowest pressure. As examples of actual data, we present time series of surface observations from four stations in Fig. 13; recorder traces of pressure and wind at College Park, Maryland (CPK) are shown in Fig. 14. This effect is seen at CPK and at

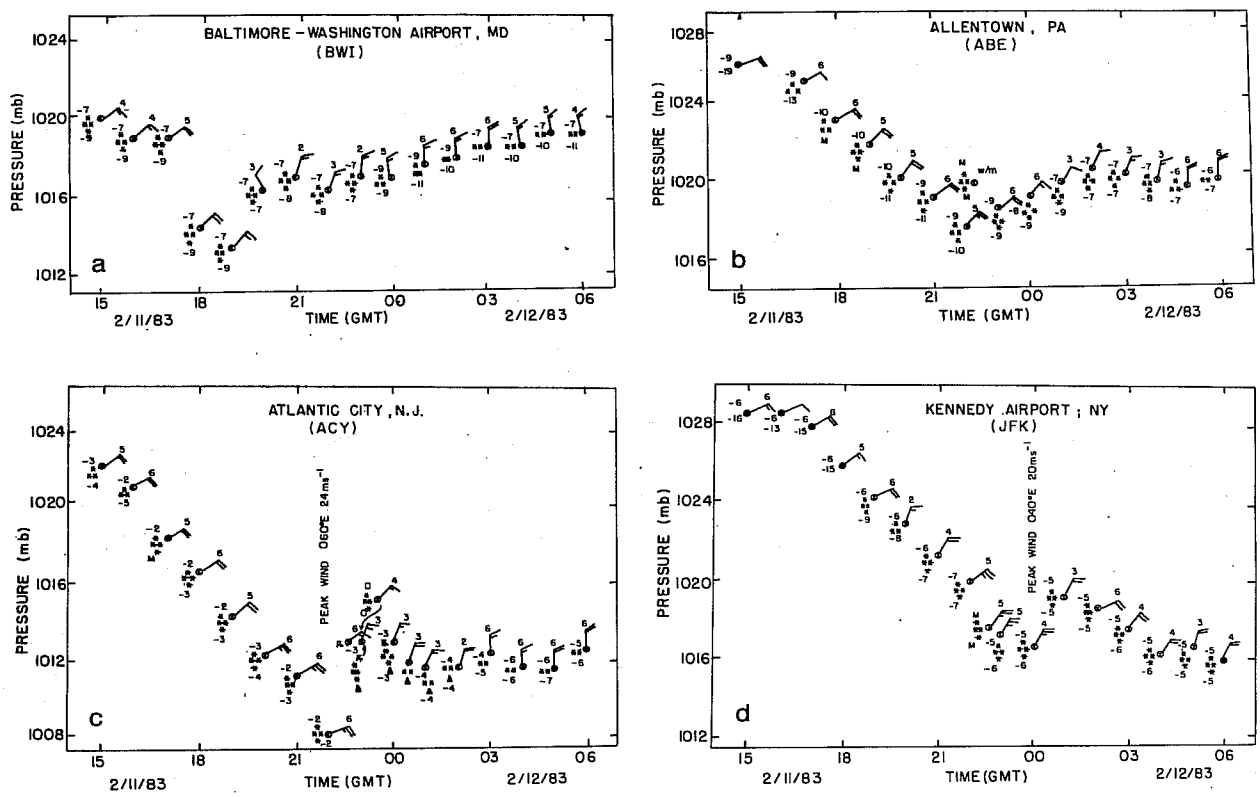

FIG. 13. Time section of hourly and special observations as a function of mean sea level pressure (mb) (a) for BWI; (b) for ABE; (c) for ACY; (d) for JFK. Plotting model as in Fig. 1.

all stations in Fig. 13. Similar gusty easterly winds were reported in the cases studied by Brunk (1949), Ferguson (1967) and Bosart and Cussen (1973).

Almost all stations affected by the wave show a response attributable to the intense pressure gradient associated with the rapid pressure rise. Southwesterly winds, as suggested by Fig. 12, are not observed; rather, owing to the strong basic current, the northeasterlies weaken and back, as far as northwest in some instances (cf. BWI in Fig. 13 and CPK in Fig. 14.) The direction of the change is southwesterly, for the most part, with magnitude undergoing an evolution like that of the pressure amplitude shown in Fig. 11, except that the strongest wind shifts occur between 20 and 22 GMT, 2-3 h earlier than the greatest pressure rises (compare curve B in the lower panel of Fig. 11). The positions of the maximum hourly wind shift match closely those of the maximum hourly rise. In view of the periodicity, the end of the hour of maximum change is usually approximately the time of extreme value. Thus Fig. 12 is comfirmed.

4.1b Cloud and precipitation

The descent and adiabatic warming in the region of pressure fall should tend to discourage precipitation and dissipate cloud. Brunk (1949) notes diminished thunderstorm activity at the time of lowest pressure in his case study, with largest pressure amplitude in a region of little or no rain. In Ferguson's (1967) case, the data shows a cessation of precipitation during the time of rapidly falling pressure and strong northeasterly wind, while Bosart and Cussen (1973) show an end of precipitation as the

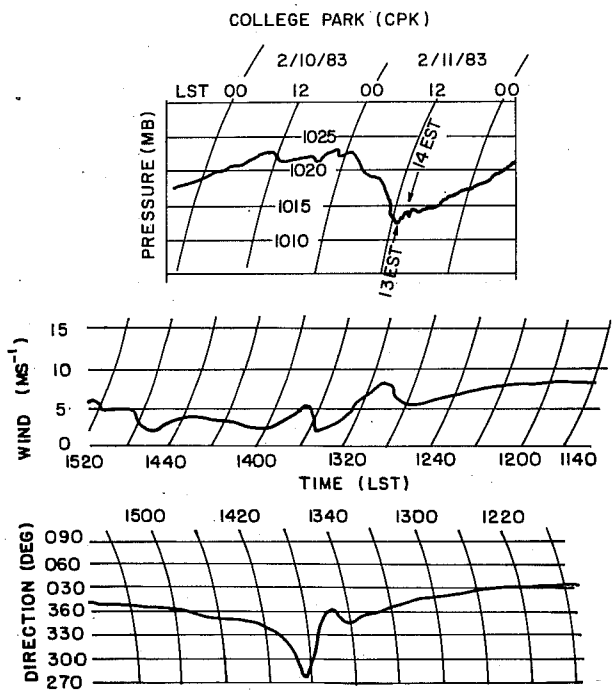

FIG. 14. Detailed data for College Park, Maryland (CPK). Barogram at top and wind speed and direction at center and bottom, respectively.

trough of low pressure passes.

Conversely, ascent occurs in the region of pressure rise in Fig. 12 and in the aforementioned instances, as in Pothecary's (1954) case, there was evidently a resumption of precipitation or development of cloud. A similar phenomenon was noted by Uccellini (1975).

In the present case the entire system is embedded in a heavy snowstorm, so that the vertical displacement due to the wave is superposed on substantial ascent of larger scale, as shown by Sanders and Bosart (1985a). It is not possible to infer anything systematically from the hourly observations of snow intensity because, as seen in Fig. 13, it is heavy throughout. For every supportive change in visibility there is a contradictory one. Perhaps this is to be expected given the dilatory fall velocities of crystals, the strong winds at low levels, and the difficulty in distinguishing between falling and blowing snow.

Direct MIT Doppler radar evidence of the effect of the wave was presented, however, by Sanders and Bosart (1985b). The leading fall area could not be detected clearly on radar in the MIT area, as this feature was propagating out of the precipitation shield at the time. The enhancement of updraft with the passage of the rise area is clearly shown around 03-04 GMT in their Fig. 11b, as is suppression of ascent 2 h later as the trailing falls moved by. The integrated condensation rate dropped by a factor of 2.4 during this episode. The snowfall rate at the ground during the storm was reported as heavy only in the two hours following the wave-enhanced ascent, but equally low

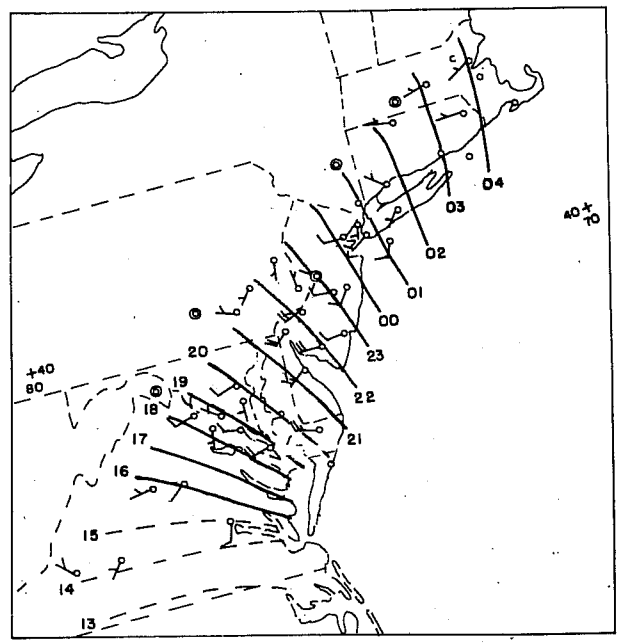

FIG. 15. Isochrones of the time (GMT) at the end of the hour of greatest vector wind shift. Dashed line indicates the ill-organized phase. One full (half) represents 5 m s^{-1} (2.5 m s^{-1}) magnitude of vector shift.

visibility was recorded at other times, due to a mixture of blowing and falling snow. There was no report of enhanced snow accumulation on the ground that could be attributed to the wave. Thus it seems that the undeniable effect of the wave on the overhead condensation rate is not clearly related to ground accumulation, owing to complexity of physical process and to difficulty of observation. [Uccellini (personal communication, 1985) observed at least three distinct bursts of snowfall at a point between DCA and BWI so the difficulty of determining precipitation rates must not be underestimated.]

A broader view of the impact of the wave on the higher cloudiness can be obtained from Fig. 16. Since the winds in the upper troposphere are strong southwesterlies, the appearance of cold tops in southern New Jersey at 20 GMT (Fig. 16d) and in southern New England at 02 GMT (Fig. 16f) represent growth attributable to the wave, rather than translation of existing cloud. Similar evidence is provided by Sanders and Bosart (1985b). The wave propagates entirely through the high cloud shield, however, and its effect is not dramatic.

Mention should also be made that the heavy snow region in Fig. 16, which initially lies near the southern edge of the highest and coldest cloud, is gradually left behind by the faster moving cold cloud mass. This is entirely consistent with the idea of a sloping snyoptic scale updraft in middle latitude cyclones as has been documented by numerous investigators (e.g., see Bjerknes, 1919; Green et al., 1966; Carlson, 1980). We add that the embedded patchiness of the individual cloud top elements

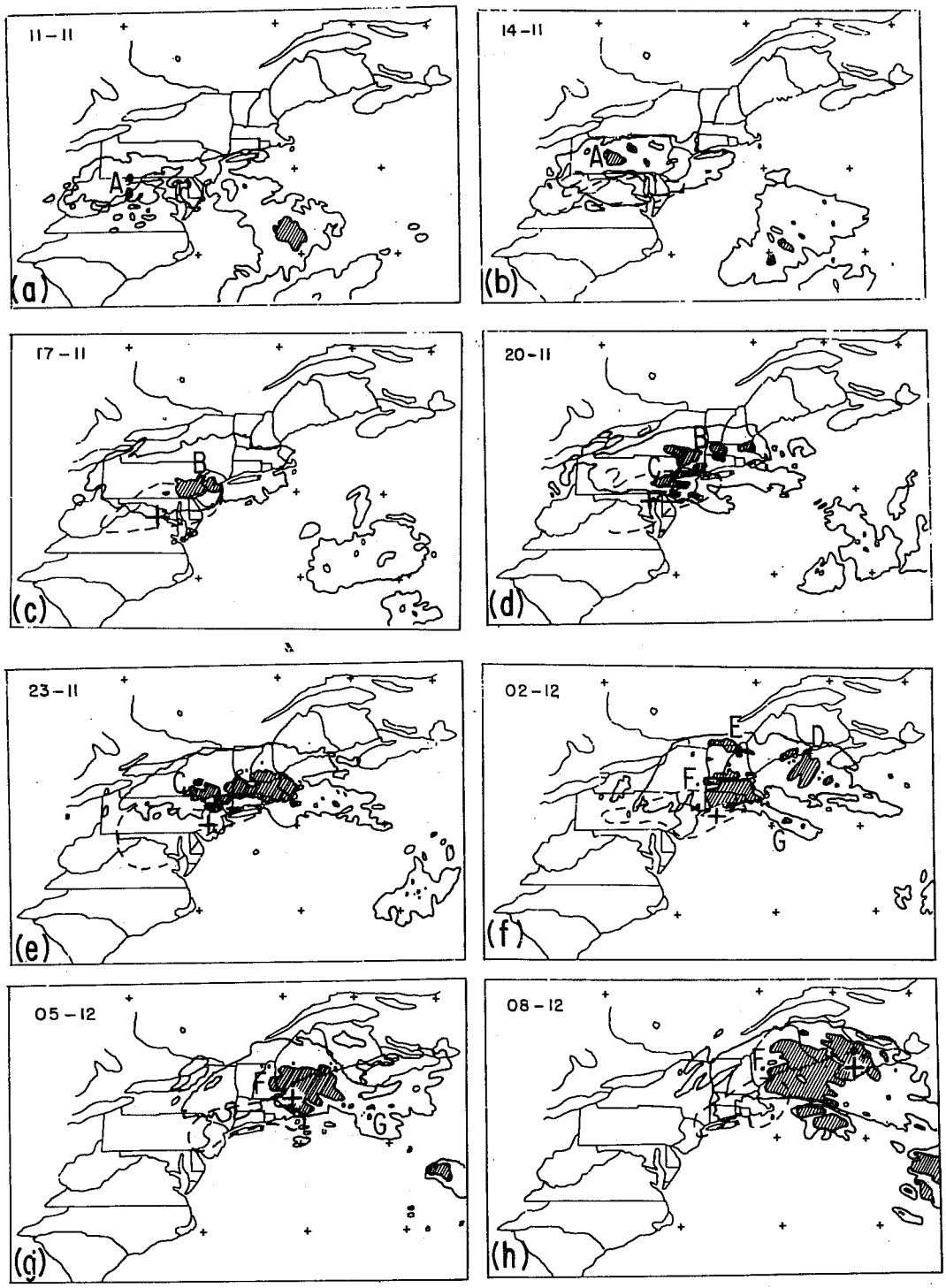

FIG. 16. Outlines of areas of cloud-top temperatures lower than −53°C (shaded) and −42°C (not shaded) as estimated from GOES satellite infrared imagery, 3 h intervals (a) beginning 11 GMT 11 February 1983 and (h) ending 08 GMT 12 February 1983. Area of moderate or heavy snow enclosed by dashed line. Letters denote discrete areas of cold cloud. Plus sign indicates position of maximum one-hour pressure rise, ending at hour of map, for high amplitude gravity wave.

is a manifestation of smaller scale processes in the storm dynamics. We note without further comment that quantitative precipitation forecast schemes based primarily upon cloud temperature characteristics will fail miserably in these situations.

4.1c The Thunderstorms

A striking effect produced by the wave was the electrical activity discussed above in relation to the pressure osillations. Thunder was reported at numerous surface stations.

The actual lightning locations are shown in Fig. 17. Positive polarity is indicated along with the time of the surface wind shift as it passed through each lightning cluster. It seems significant that all the SUNYA groundflash observations (except an early one unrelated to the gravity wave) occur over land or within 25 km of the coast. Close examination shows that about 60% of the 69 flashes are clustered in one of four more-or-less discrete episodes. All of these clusters, except perhaps the one in east-central New Jersey, occur along or near the south edge of the deep cloud area, where it is intersected by the surface windshift line. The exception occurs in the zone of cloud buildup to the south, but the thunderstorms are also along the windshift line.

Each localized region of electrical activity tends to remain in place for a few hours rather than move with the winds aloft or propagate with the gravity wave. In the areas described above, the last flashes occur at 2305 GMT, at 0105 GMT, at 0334 GMT, at 0733 GMT and at 0352 GMT, respectively. Thus, these

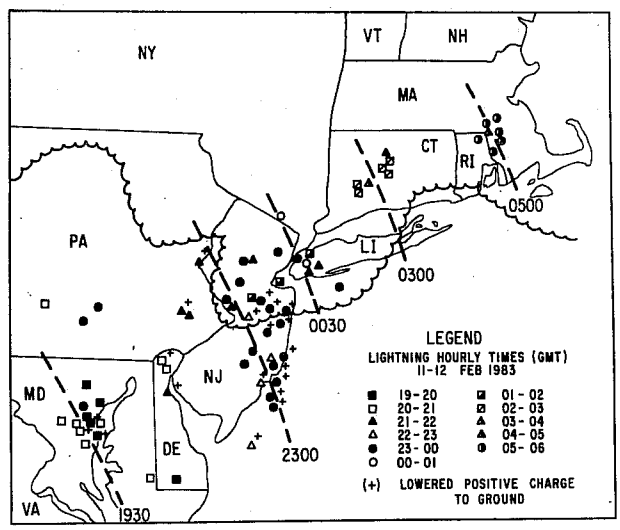

FIG. 17. Lightning locations from the SUNYA network for the period 18 GMT 11 February through 06 GMT 12 February 1983. Hourly time sequence according to legend. Appropriate wind shift lines from Fig. 7 are superimposed. Scalloped line encloses region of continuous cloud top temperatures $< -32°C$ at 00 GMT 12 February 1983.

thundery groups, once triggered, appear more fastened to something on the earth's surface than to something in the atmosphere.

The exceptional southward-extending thunderstorm outbreak in New Jersey is distinctive also in that all flashes south of the northernmost ones carry positive charge to the ground, whereas all subsequent flashes to the north and east lower negative charge. What is unusual about these storms?

The nominal 00 GMT sounding from ACY appears in Fig. 18. The balloon was probably released shortly after 23 GMT, just after the start of the thunderstorm acitivty and on its southwest edge, but thunder is heard at the station at 23 and 00 GMT. There is little instability for upright convection, with potential instability indicated only for the layer between 680 and 500 mb. The cloud top is indicated at 590 mb at a temperature of $-14^{o}C$, consistent with the cloud-top temperatures in the region south of the deep cloud. Now if the unsaturated air at 540 mb were raised by the gravity wave to its lifting condensation pressure and temperature of 460 mb and $-30^{o}C$, then air rising in an undilute cumulus updraft from 680 mb would have $2^{o}C$ of buoyancy at this level but would be unable to penetrate much farther, owing to the stability of the ambient atmosphere above.

Thus the thunder-producing cumulonimbus would be weak examples with tops warmer than those of most thunderstorms consistent however, with the cloud-top temperatures indicated in Fig. 16e. The available evidence, therefore, suggests that these

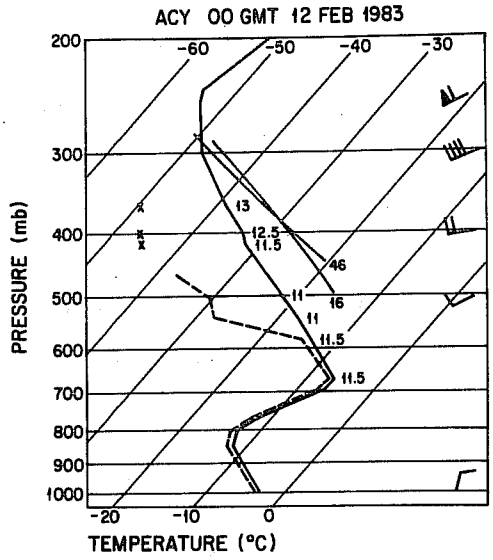

FIG. 18 Sounding from ACY 00 GMT 12 February. Temperature and dew point shown by solid and dashed lines, respectively. Plotted values denote wet-bulb potential temperature (°C). Thin lines represent 46°C dry adiabat and moist adiabat for 16°C wet-bulb potential temperature. Partial winds for IAD (ACY wind equipment failed) with pennant, full barb and half barb denoting 25, 5 and 2.5 m s^{-1}, respectively.

relatively mild, shallow thunderstorms lower positive charge to the ground. A substantial fraction of thunderstorms southwest of ACY lower positive charge as well, but Fig. 16 and Fig. 17 (coldest tops tend to be north of the region where positive charge is lowered to ground) and data presented by Sanders and Bosart (1985b), suggest that these, but not those northeast of the New Jersey outbreak, may be shallow. Even the latter, however, are likely weak, to judge from the instability of the ambient atmosphere, so it seems that cloud-top temperature, rather than updraft vigor, may determine the electrical character, if we may hazard a frail conjecture. The question is of practical as well as scientific interest, because of the potential disruption of power grids and transmission facilities by positive flashes which tend to exhibit higher peak currents than negative flashes (Brook et al., 1982).

Takeuti et al., (1978) have reported that winter thunderstorms along the Hokuriku coast of Japan often lower positive charge to ground. Brook et al., (1982) noted a strong correlation between the fraction of positive ground flashes and the vertical shear in the cloud layer. They reasoned that the presence of a sheared environment enabled positive streamers from the upper region of the cloud to reach the surface rather than the negatively charged regions in the lower part of the cloud as would be the case in an unsheared environment. They suggested a shear threshold of 1.5 m s^{-1}/km for the appearance of positive strokes to ground. While the absence of wind information at ACY (Fig. 18) precludes a determination of the actual shear in the

present case the results of Sanders and Bosart (1985a) indicate that the geostrophic shear is well above this threshold.

An alternative explanation of the electrification might appeal to the updrafts, and especially the strong shears, in the frontal circulation or perhaps in "slant-wise convection" resulting from symmetric instability, which were evidently present in this storm. If this were the agent, however, the clusters of activity would have occurred randomly along the baroclinic zone, rather than in close relation to the gravity wave, as observed.

4.2 Summary of wave-structure and origin

The wave activity was initiated just ahead of , and to the left of, the track of a major cyclone which was responsible for the megalopolitan snowstorm of 11-13 February 1983.

Hourly changes of sea level pressure up to several millibars accompanied the system, which first resembled a classic wave of depression. The pressure rises then increased to produce a wave of elevation, which was finally followed by a wake depression. The system propagated northeastward in the coastal region at 15m s^{-1} accelerating to more than 25 m s^{-1}, against an increasing northeasterly flow at low levels. Its scale in the direction of propagation contracted upon organization to about 100 km, then expanded to more than 400 km as it accelerated during the remainder of the 12 hours over which it could be reliably tracked. The system period increased slowly from somewhat less to somewhat more than 3 hours.

Surface northeasterlies increased and became gusty with the

approach of the first pressure falls, reaching a maximum at the pressure trough, then abruptly weakened and backed as strong pressure increases were observed. The behavior was in accord with a simple model of a gravity wave.

Strong fluctuations in column total condensation rate and radar reflectivity occurred with the passage of the wave, in qualitative agreement with the simple model. The effect could not be reliably detected in the surface snowfall observations, however, owing to difficulty in determining short-term fluctuations of snowfall rate in strong winds. Modest convective cloud buildups were triggered by the wave in potentially unstable air where a dry intrusion in middle-tropospheric levels had removed a continuous layer of deep high cloud.

Electrical activity was initiated by wave passage, but in discrete, sporadic clusters at intervals of about 3 hours. Each cluster tended to remain geographically fixed for 2-4 hours after initiation. The clusters occurred principally near the intersection of the gravity wave cloud along the north edge of the dry intrusion. These flashes carried predominantly negative charge to ground. A unique cluster of flashes developing from clouds with relatively low, warm, tops, growing in the northern periphery of the dry intrusion, lowered exclusively positive charge to ground.

The first disorganized gravity-wave activity developed in the presence of modest convection just south of the mass of deep high cloud, and also beneath the region of likely wave generation in a strong shear zone beneath an advancing jet streak.

The singular-appearing large-amplitude wave became organized subsequently in a transient meridionally oriented zone of strong frontogenetical forcing that did not succeed in producing a surface front. Rather, the wave appeared as the northern extension of a front farther south reaching down to the low center.

The propagation speed of the system was in reasonable accord with the gravity-wave model of Lindzen and Tung (1976), but the theoretical speed was a few m s^{-1} slower than observed. Uncertainties in the interpretation of the structure of the ambient atmosphere and in the interpretation of the solitary aspects of the wave were sufficient to account for the discrepancies. We conclude that the system represented a ducted gravity wave propagating in a layer of large stability beneath an elevated layer of small Richardson number containing a critical level. Whether the accompanying convection and enhancement of condensation heating represented a forcing effect on the wave is unknown because of uncertainties concerning its vertical structure, but circumstantial evidence indicates that the answer is probably yes.

Bosart and Seimon (1987) have recently studied another example of a long-lived large amplitude gravity wave in conjunction with cyclogenesis over the eastern United States in February 1984. For example, a spectacular pressure fall of almost 14 mb in 35 minutes was observed at Raleigh-Durham, North Carolina as the wave passed. Noteworthy aspects of this case include: (1) wave origin and intensification to the rear of a

line of convection propagating eastward to the coast and (2) cloud dessication and disruption after wave passage. Bosart and Seimon (1987) noted that the wave amplified along the eastern slopes of the Appalachian Mountains and became very intense as it crossed the cold air damming region between the mountains and the coast. A strong low-level thermal inversion could be found within the cold air damming region. Agreement between the theoretical phase velocity required to satisfy the Lindzen and Tung (1976) ducted gravity wave model and observation was reasonably good.

The wave genesis mechanism(s) could not be isolated convincingly. Both shearing instability in the form of strong vertical wind shear and Richardson number 0.5 and geostrophic adjustment in the presence of large upper level divergence ahead of an advancing jet streak were present. The gravity wave formed in a region where the moist potential vorticity (and moist potential vorticity tendency) was negative. The criteria for symmetric instability, $[(\eta/f)Ri < 1]$ where η is the absolute vorticity, f is the coriolis parameter and Ri the Richardson number, was also satisfied in the wave origin region. Kerry Emanuel (personal communication) has also suggested that wave growth might be attributable to resonance in a weakly symmetrically unstable environment. It should also be noted that wave origin occurred where one would expect to find the trailing wake depression associated with a propagating squall line. Given the presence of a very stable boundary layer (the wave formed north of a quasi-stationary frontal boundary) it is possible that

significant surface pressure perturbations were triggered by the adiabatic descent of air in the wake of the squall line. Once formed, wave maintenance was favored by the existence of a well defined wave guide (thermal inversion) from the mountains to the coast.

5. Coastal frontogenesis processes

Coastal fronts are found in the United States along the Atlantic coast (particularly New England and from the Delmarva Peninsula to Georgia) and the Texas coast. The observed structure of coastal fronts can be found in papers by Bosart et al., (1972), Bosart (1975), Marks and Austin (1979), and Bosart (1984). The coastal front is a mesoscale phenomenon. The typical coastal front is shallow ($\sim$500m) and is confined to the boundary layer. It may extend anywhere from 200 to 1000 km along the coast while the cross frontal width averages 10 km. The temperature contrast across the 10 km frontal zone may reach 10^{o}C. Temperature changes of this magnitude across 1 km have been measured with instrumented cars traversing New England coastal fronts.

The coastal front often marks the boundary between frozen and non-frozen precipitation. Precipitation tends to be heavier on the cold side of the frontal boundary in response to a thermally direct frontogenetical circulation about the front. The papers by Bosart (1981) and Bosart and Lin (1984) highlighted the importance that the coastal front played in the development of the Presidents' Day storm of February 1979 along the US Atlantic coast. In that storm the coastal front formed along the coast in

a deep, but very cold, onshore easterly flow regime. The air moving westward toward the coast was of recent arctic origin. The air was funneled southward and then westward around a massive 1050 mb anticyclone situated over the northeastern US. Sensible and latent heat fluxes from the sea surface warmed, moistened and destabilized the arctic air mass. Meanwhile, very cold air funneling southward east of the Appalachian Mountains became juxtaposed alongside the onshore easterly flow. The resulting line of large temperature contrast marked the coastal front boundary. Bosart (1981) and Uccellini et al. (1984, 1985) showed how a weak cyclonic disturbance formed along the coastal front boundary east of Georgia and then explosively deepened as a potent short wave trough aloft reached the coast from the west.

The coastal front boundary serves as a locus of frontogenesis, moisture convergence and cyclonic vorticity production. Keshishian and Bosart (1987) and Clark (1983) showed these effects in a study of extended frontogenesis and cyclogenesis during December 1981. Nondeepening cyclones, given the name zipper lows, would propagate northeastward along the coastal front boundary. Geostrophic frontogenesis would tighten the temperature gradient ahead of a zipper low. The absence of significant cold advection in the wake of the zipper low left a baroclinic zone (in the presence of residual moisture) in place along the coast. Thus the atmosphere is "preconditioned" for a later cyclogenetic response in that a moist baroclinic zone in the presence of reduced static stability and enhanced boundary layer cyclonic vorticity is produced along the coastal zone. It

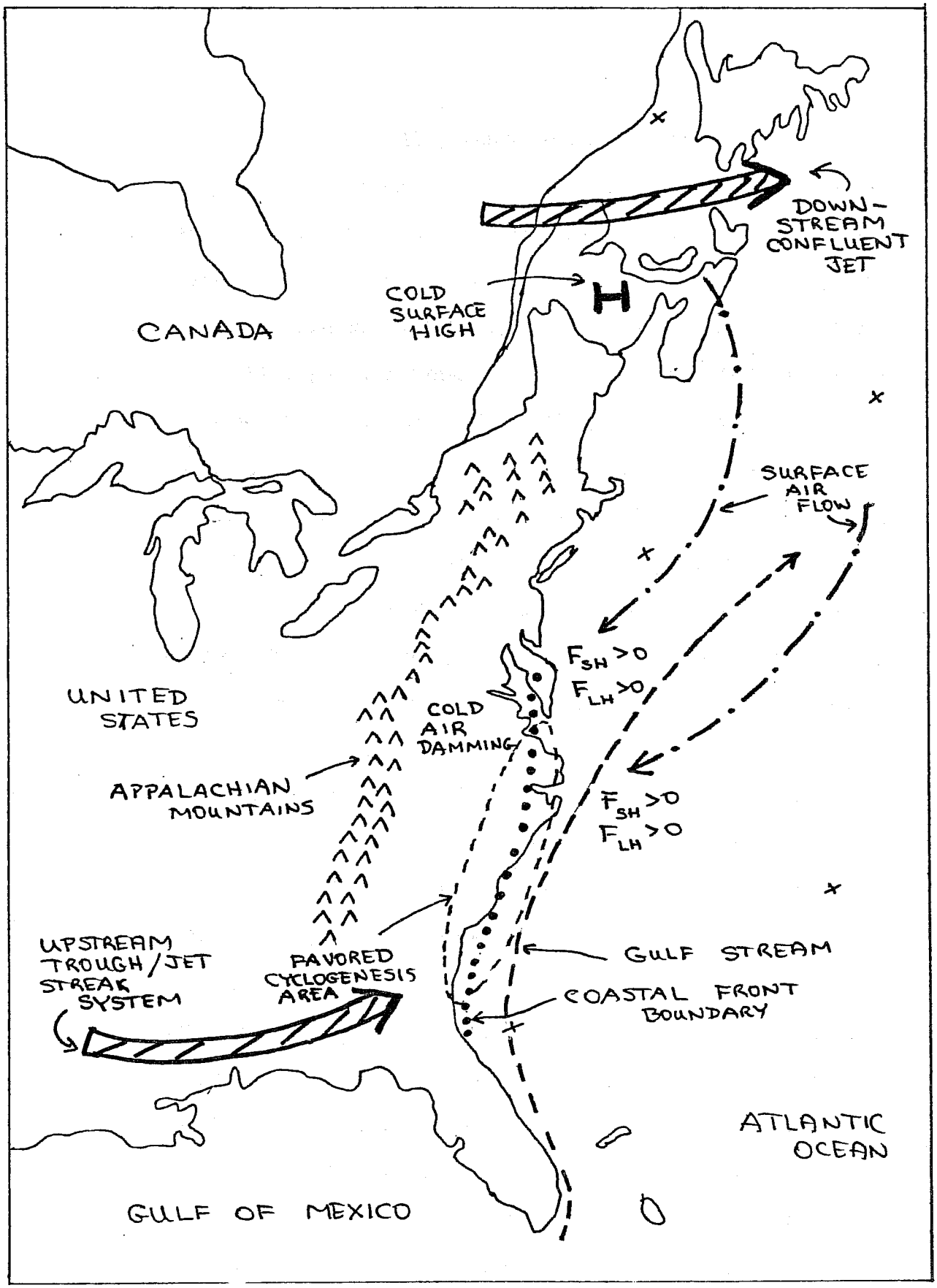

Fig. 19 Schematic of physical processes important to explosive cyclogenesis along the East Coast of the United States.

was shown by Keshishian and Bosart (1987) that rapid cyclogenesis could ensue when the updraft region of a mobile short wave trough aloft became superimposed over the "preconditioned" lower troposphere.

These ideas are summarized in schematic form in Fig. 19. A key point to appreciate from Fig. 19 is that the mesoscale surface coastal frontogenesis is crucially dependent upon the larger scale synoptic configuration. Bell (1987, personal communication) composited eleven cases of New England coastal frontogenesis (associated with major Atlantic coast cyclogenesis) from the cases used by Bosart (1975). He showed that the onset of coastal frontogenesis occurred with the passage of the 500 mb ridge line and the beginning of appreciable warm air advection at 850 mb. The downstream ridge is enbedded in a confluent flow pattern at 500 mb which supports the cold anticyclone over the northeastern United States and Canada. Cold air is driven southwestward to the east of the Appalachian Mountains and the thermal gradient is tightened along the coast. The approach of an upstream trough helps to induce cyclogenesis (it may be secondary cyclogenesis) along the enhanced coastal baroclinic zone. Cyclone spin-up is especially favored in a vorticity rich highly convergent lower troposphere.

In the seminar these processes were illustrated by means of the explosive cyclogenesis event of 0000 GMT 17 February 1974 along the US Carolina coast. Coastal frontogenesis began around 1200 GMT 16 February and became quite intense over the next 6-12 h. Surface frontogenesis rates (computed from subjective

analyses on a 1^{o} latitude-longitude mesh) averaged $35\text{-}40 \times 10^{-10}$ $^{o}C\ m^{-1}\ s^{-1}$ along the coastal strip in advance of the developing cyclone. At 1800 GMT 16 February the relative vorticity averaged $10\text{-}15 \times 10^{-5}\ s^{-1}$ over the same coastal strip while the computed local vorticity tendency was $8\text{-}13 \times 10^{-9}\ s^{-2}$ ($\sim 10f\ day^{-1}$). The corresponding moisture flux divergence amounted to $\sim -35 \times 10^{-5}\ g\ kg^{-1}\ s^{-1}$. By 0000 GMT 17 February the computed vorticity tendency and moisture flux divergence had doubled while the frontogenesis rate remained unchanged. The surface sensible heat flux (computed by the bulk aerodynamic method) averaged 450 Wm^{-2} ahead of the track of the now rapidly deepening cyclone.

Aloft, the quasi-geostrophic forcing was significant throughout the troposphere but was largest at 850 mb. Likewise, the 850 mb geostrophic frontogenesis (proportional to $\vec{Q} \cdot \nabla\theta$) exhibited a well defined maximum ($\sim 50\text{-}60 \times 10^{-15}\ K^{2}\ m^{-2}\ s^{-1}$) ahead of the track of the surface cyclone at 0000 GMT 17 February. Frontogenesis was also computed at 500 mb but only half as much as at 850 mb.

In summary the explosive cyclogenesis event of 16-17 February 1974 involved a complex interaction of synoptic and mesoscale circulations. The synoptic scale forcing was strong but hardly extraordinary. Upper air troughs of that intensity (strongest 500 mb winds of $\sim 40\ ms^{-1}$ and temperatures of $-20^{o}C$) routinely cross the coast in winter. The surface response to the synoptic scale forcing, however, was extraordinary. It is tempting to conclude that the coastal frontogenesis process

preconditioned the lower troposphere for an extraordinary response by creating a highly moist, vorticity rich baroclinic environment in which rapid cyclone spin-up could take place as the updraft region associated with the trough aloft swept over the coastal baroclinic zone. Appreciable oceanic surface sensible and latent heat fluxes ahead of the cyclone track may have further augmented the cyclogenesis process through boundary layer warming and moistening and resultant destabilization. It is also interesting that the observed cyclone deepeded 15 mb (973 to 958 mb) in the three hour period ending 0900 GMT 17 February as the storm traversed a 100 km warm Gulf Stream ring in which the water temperature reached 24°C.

Acknowledgment

The SUNYA research presented in this paper has been supported by National Science Foundation grants ATM 802655702, ATM 8311106 and ATM 8445006. The text was prepared by Celeste Iovinella.

6. References

Anthes, R.A., Y.-H. Kuo and J.R. Gyakum, 1983: Numerical simulations of a case of explosive marine cyclogenesis. **Mon. Wea. Rev., 111**, 1174-1188.

Atkinson, B.W., 1981: Meso-scale Atmospheric Circulations, Academic Press, New York, NY, 495 pp.

Bennetts, D.A., and B.J. Hoskins, 1979: Conditional symmetric instability--a possible explanation for frontal rainbands. **Quart. J. Roy. Meteor. Soc., 105**, 945-962.

Bjerknes, J., 1919: On the structure of moving cyclones. **Geofys. Publikajoner, Norske Videnskaps-Akad., 1**, 1-8.

Bosart, L.F., 1975: New England coastal frontogenesis. **Quart. J. Roy. Meteor. Soc., 101**, 957-978.

------, 1981: The Presidents' Day Snowstorm of 18-19 February 1979: A subsynoptic scale event. **Mon. Wea. Rev., 109**, 1542-1566.

------, 1984: The Texas coastal rainstorm of 17-21 September 1979: An example of synoptic-mesoscale interaction. **Mon. Wea. Rev., 112**, 1108-1133.

------, C.J. Vaudo and J.H. Helsdon, Jr. 1972: Coastal frontogenesis. **J. Appl. Meteor., 11**, 1236-1258.

------, and J.P. Cussen, Jr., 1973: Gravity wave phenomena accompanying East Coast cyclogenesis. **Mon. Wea. Rev., 101**, 446-454.

------, and S.C. Lin, 1984: A diagnostic analysis of the Presidents' Day Storm of February 1979. **Mon. Wea. Rev., 112**, 2148-2177.

------, and F. Sanders, 1986: Mesoscale structure in the megalopolitan snowstorm of 11-12 February 1983. Part III: A large-amplitude gravity wave. **J. Atmos. Sci., 43**, 924-939.

------, and A. Seimon, 1987: An unusually intense long-lived large-amplitude gravity wave. **Mon. Wea. Rev.**, paper conditionally accepted.

Brooks, C.F., and I.I. Schell, 1950: Forecasting heavy snowstorms at Blue Hill (Boston), Mass. **Bull. Amer. Meteor. Soc., 31**, 131-133.

Brook, M., M. Nakano and P. Krehbiel, 1982: The electrical structure of the Hokuriku winter thunderstomrs, **J. Geophys. Res., 87 (C2)**, 1207-1215.

Browning, K.A., (Editor) 1982: Nowcasting, **Academic Press, New York, NY**, 256 pp.

Brunk, I., 1949: The pressure pulsation of 11 April 1944. **J. Meteor., 6**, 181-187.

Carlson, T.B., 1980: Airflow through midlatitude cyclones and the comma cloud pattern. **Mon. Wea. Rev., 108**, 1498-1509.

Clark, D.A., 1983: A comparative study of coastal frontogenesis. Master's thesis, Dept. of Meteor., MIT, Cambridge, MA, USA 86 pp.

Durran, D.R. and J.B. Klemp, 1982: On the effects of moisture on the Brunt-Vaisala freguency. **J. Atmos. Sci., 39**, 2152-2158.

Eliassen, A., 1959: The formation of fronts in the atmosphere, **The Atmosphere and the Sea in Motion,** , B. Bolin, Ed., The

Rockefeller Institute Press, 277-287.

Emanuel, K.A., 1983a: The Lagrangian parcel dynamics of moist symmetric instability. **J. Atmos. Sci., 40**, 2368-2376.

------, 1983b: On assessing local conditional symmetric instability from atmospheric soundings. **Mon. Wea. Rev., 111**, 2016-2033.

------, 1985: Frontogenesis in the presence of low moist symmetric stabilty. **J. Atmos. Sci., 42**, 1062-1071.

Eom, J., 1975: Analysis of the internal gravity wave occurrence of April 19, 1970 in the Midwest. **Mon. Wea. Rev., 103**, 217-226.

Ferguson, H.L., 1967: Mathematical and synoptic aspects of a small-scale wave disturbance over the lower Great Lakes area. **J. Appl. Meteor., 6**, 523-529.

Green, J.S.A., R.H. Ludlam and J.F.R. McIlveen, 1966: Isentropic relative-flow analysis and the parcel theory. **Quart J. Roy. Meteor. Soc., 92**, 210-219.

Gyakum, J.R., 1983a: On the evolution of the QE-II storm. Part I: Synoptic aspects. **Mon. Wea. Rev., 111**, 1137-1155.

------, 1983b: On the evolution of the QE-II storm. Part II: Dynamic and thermodynamic structure, **Mon. Wea. Rev., 111**, 1156-1173.

Herzegh, P.H., and P.V. Hobbs, 1980: The mesoscale and microscale structure and organization of clouds and precipitation in midlatitude cyclones. Part II: Warm frontal clouds. **J. Atmos. Sci., 37**, 597-611.

Heymsfield, G.M., 1979: Doppler radar study of warm frontal region. **J. Atmos. Sci., 36**, 2093-2107.

Hoskins, B.J., and F.P. Bretherton, 1972: Atmospheric frontogenesis models: Mathematical formulation and solution. **J. Atmos. Sci., 29**, 11-37.

Houze, R.A., Jr., S.A. Rutledge, T.J. Matejka and P.V. Hobbs, 1981: The mesoscale and microscale structure and organization for clouds and precipitation in midlatitude cyclones. Part III: Air motions and precipitation growth in a warm-frontal rainband. **J. Atmos. Sci., 38**, 639-649.

Keshishian, L.G. and L.F. Bosart, 1987: A case study of extended East Coast frontogenesis, **Mon. Wea. Rev., 115**, 100-117.

Lai, C.-C. and L.F. Bosart, 1987: Trough Phasing: An example for a difficult forecast problem. Submitted for publication to **Mon. Wea. Rev.**.

Lindzen, R.S., and K.K. Tung, 1976: Banded convective activity and ducted gravity waves. **Mon. Wea. Rev., 104**, 12, 1602-1617.

Marks, F.D., and P.M. Austin, 1979: Effects of the New England coastal front on the distribution of precipitation. **Mon. Wea. Rev. 107**, 53-67.

Namias, J., and P.F. Clapp, 1949: Confluence theory of the high tropospheric jet stream. **J. Meteor., 6**, 330-336.

Orville, R.E., R.W. Henderson and L.F. Bosart, 1983: An east coast lightning detection system. **Bull. Amer. Meteor. Soc., 64**, 1029-1037.

Pecnick, M.J., and J.A. Young, 1984: Mechanics of a strong subsynoptic gravity wave deduced from satellite and surface observations. **J.Atmos. Sci., 41**, 1850-1862.

Pothecary, I.J.W., 1954: Short-period variations in surface pressure and wind. **Quart. J. Roy. Meteor. Soc., 80**, 395-401.

Rasmussen, E., 1985: A case study of a polar low development over the Barents Sea. **Tellus, 37A**, 407-418.

Ray, P.S., (Editor), 1986: Mesoscale Meteorology and Forecasting, **Amer. Meteor. Soc.**, Boston, MA, USA 793 pp.

Reed, R.J., 1979: Cyclogenesis in polar airstreams, **Mon.Wea. Rev., 107**, 38-52.

------, and M.D. Albright, 1986: A case study of explosive cyclogenesis in the eastern Pacific. **Mon. Wea. Rev., 114**, 2297-2319.

Sanders, F. and L.F. Bosart, 1985a: Mesoscale structure in the megalopolitan snowstorm of 11-12 February 1983. Part I: Frontogenetical forcing and symmetric instability. **J. Atmos. Sci., 42**, 1050-1061.

------, and------, 1985b: Mesoscale structure in the megalopolitan snowstorm of 11-12 February 1983. Part II: Doppler radar study of the New England snowband. **J. Atmos. Sci., 42**, 1398-1407.

Saywer, J. S., 1956: The vertical circulation at meteorological fronts and its relation to frontogenesis. **Proc. Roy. Soc. London, A234**, 246-262.

Shapiro, M.A., L.S. Fedor and T. Hampel, 1987: Research aircraft measurements within a polar low over the Norwegian Sea. **Tellus, 39A**, Paper in press.

Takeuti, T., M. Nakano, M. Brook, D.J. Raymond and P. Krehbiel,

1978: The anomalous winter thunderstorms of the Hokuriku Coast. **J. Geophys. Res., 83 C5**, 2385-2394.

Thorpe, A.J. and K. Emanuel, 1985: Frontogenesis in the presence of small stability to slantwise convection. **J. Atmos. Sci.**, 42 1809-1824.

Tracton, M.S., 1973: The role of cumulus convection in the development of extratropical cyclones. **Mon. Wea. Rev., 101**, 573-593.

Uccellini, L.W., 1975: A case study of apparent gravity wave initiation of severe convective storms. **Mon. Wea. Rev., 103**, 497-513.

------, 1986: The possible influence of upstream upper-level baroclinic processess on the development of the QE II storm. **Mon. Wea. Rev., 114**, 1019-1027.

------, P.J. Kocin, R.A. Petersen, C.H. Wash and K.F. Brill, 1984: The Presidents' Day cyclone of 18-19 February 1979: Synoptic overview and analysis of the subtropical jet streak influencing the pre-cyclogenetic period. **Mon. Wea. Rev., 112**, 31-55.

------, D. Keyser, K.F. Brill and D.H. Wash, 1985: The Presidents' Day cyclone of February 1979: Influence of upstream trough amplification and asociated tropopause folding on rapid cyclogenesis. **Mon. Wea. Rev., 113**, 962-988.

------, and S.E. Koch, 1987: The synoptic setting and possible energy sources for mesoscale wave disturbances. **Mon. Wea. Rev., 115**, 721-729.

Wagner, A.J., 1962: Gravity wave in New England, April 12, 1961. **Mon. Wea. Rev., 90**, 431-436.

Figures

Figs. 1, 2: Source: Adrian Simmons, ECMWF

Figs. 3, 4: Source: Richard E. Orville, SUNY - Albany

Figs. 5-10: Sanders and Bosart (1985a)

Figs. 11-18: Bosart and Sanders (1986)